



Published in final edited form as:

*Nat Immunol.* 2023 December ; 24(12): 2108–2120. doi:10.1038/s41590-023-01667-y.

## Selective IL-27 production by intestinal regulatory T cells permits gut-specific regulation of T<sub>H</sub>17 cell immunity

Chia-Hao Lin<sup>1</sup>, Cheng-Jang Wu<sup>1</sup>, Sungrim Cho<sup>1</sup>, Rasika Patkar<sup>1</sup>, William J. Huth<sup>1</sup>, Ling-Li Lin<sup>1</sup>, Mei-Chi Chen<sup>1</sup>, Elisabeth Israelsson<sup>2</sup>, Joanne Betts<sup>2</sup>, Magdalena Niedzielska<sup>3</sup>, Shefali A. Patel<sup>4</sup>, Han G. Duong<sup>4</sup>, Romana R. Gerner<sup>5</sup>, Chia-Yun Hsu<sup>6</sup>, Matthew Catley<sup>3</sup>, Rose A. Maciewicz<sup>3</sup>, Hiutung Chu<sup>6,7,8</sup>, Manuela Raffatellu<sup>5,7,8</sup>, John T. Chang<sup>4,9</sup>, Li-Fan Lu<sup>1,8,10,✉</sup>

<sup>1</sup>School of Biological Sciences, University of California, San Diego, La Jolla, CA, USA.

<sup>2</sup>Translational Science and Experimental Medicine, Research and Early Development, Respiratory & Immunology, BioPharmaceuticals R&D, AstraZeneca, Gothenburg, Sweden.

<sup>3</sup>Bioscience, Research and Early Development, Respiratory & Immunology, BioPharmaceuticals R&D, AstraZeneca, Gothenburg, Sweden.

<sup>4</sup>Department of Medicine, University of California, San Diego, La Jolla, CA, USA.

<sup>5</sup>Division of Host-Microbe Systems and Therapeutics, Department of Pediatrics, University of California, San Diego, La Jolla, CA, USA.

<sup>6</sup>Department of Pathology, University of California San Diego, La Jolla, CA, USA.

<sup>7</sup>UC San Diego Center for Mucosal Immunology, Allergy, and Vaccines, Chiba University, La Jolla, CA, USA.

<sup>8</sup>Center for Microbiome Innovation, University of California, San Diego, La Jolla, CA, USA.

<sup>9</sup>Department of Medicine, Veterans Affairs San Diego Healthcare System, San Diego, CA, USA.

<sup>10</sup>Moore's Cancer Center, University of California, San Diego, La Jolla, CA, USA.

**Reprints and permissions information** is available at [www.nature.com/reprints](http://www.nature.com/reprints).

<sup>✉</sup> **Correspondence and requests for materials** should be addressed to Li-Fan Lu. [lifanlu@ucsd.edu](mailto:lifanlu@ucsd.edu).

**Author contributions**

C.-H.L. and L.-F.L. conceived and designed the project. C.-H.L., C.-J.W., S.C., R.P., W.J.H., R.R.G. and C.-Y.H. performed the experiments. C.-H.L., R.P., E.I., J.B., M.N., M.C., R.A.M., S.A.P., H.G.D. and L.-F.L. analyzed the data. L.-L.L., M.-C.C., H.C., M.R. and J.T.C. contributed critical reagents, materials and analytical tools. C.-H.L. and L.-F.L. wrote the manuscript.

**Online content**

Any methods, additional references, Nature Portfolio reporting summaries, source data, extended data, supplementary information, acknowledgements, peer review information; details of author contributions and competing interests; and statements of data and code availability are available at <https://doi.org/10.1038/s41590-023-01667-y>.

**Reporting summary**

Further information on research design is available in the Nature Portfolio Reporting Summary linked to this article.

**Extended data** is available for this paper at <https://doi.org/10.1038/s41590-023-01667-y>.

**Supplementary information** The online version contains supplementary material available at <https://doi.org/10.1038/s41590-023-01667-y>.

**Peer review information** *Nature Immunology* thanks Dan Littman and the other, anonymous, reviewer(s) for their contribution to the peer review of this work. L. A. Dempsey was the primary editor on this article and managed its editorial process and peer review in collaboration with the rest of the editorial team.

## Abstract

Regulatory T cells ( $T_{reg}$  cells) are instrumental in establishing immunological tolerance. However, the precise effector mechanisms by which  $T_{reg}$  cells control a specific type of immune response in a given tissue remains unresolved. By simultaneously studying  $T_{reg}$  cells from different tissue origins under systemic autoimmunity, in the present study we show that interleukin (IL)-27 is specifically produced by intestinal  $T_{reg}$  cells to regulate helper T17 cell ( $T_H17$  cell) immunity. Selectively increased intestinal  $T_H17$  cell responses in mice with  $T_{reg}$  cell-specific IL-27 ablation led to exacerbated intestinal inflammation and colitis-associated cancer, but also helped protect against enteric bacterial infection. Furthermore, single-cell transcriptomic analysis has identified a  $CD83^+CD62L^lo$   $T_{reg}$  cell subset that is distinct from previously characterized intestinal  $T_{reg}$  cell populations as the main IL-27 producers. Collectively, our study uncovers a new  $T_{reg}$  cell suppression mechanism crucial for controlling a specific type of immune response in a particular tissue and provides further mechanistic insights into tissue-specific  $T_{reg}$  cell-mediated immune regulation.

---

$T_{reg}$  cells control diverse types of immune responses and maintain immunological tolerance and tissue homeostasis<sup>1</sup>. Although the expression of Foxp3 as a master molecular regulator in  $T_{reg}$  cells distinguishes them from other T cell lineages, it is well recognized that, similar to conventional T ( $T_{conv}$ ) cells that they regulate,  $T_{reg}$  cells also come in different phenotypic and functional ‘flavors’<sup>2</sup>. The acquisition of helper T cell lineage-specific transcription factors in  $T_{reg}$  cells endows them with the capacities to control the corresponding immune responses in different inflammatory settings. Nevertheless, as transcription factors regulate the expression of a large number of genes, the precise effector mechanisms by which different helper T cell-specific  $T_{reg}$  cell subset control their respective type of T cell immunity have yet to be determined.

Besides the  $T_{reg}$  cell subsets that regulate different types of T cell immune responses, the presence of distinct  $T_{reg}$  cell populations in nonlymphoid tissues has also now been well appreciated<sup>3</sup>. Beyond exerting their immunoregulatory function to control local inflammation in a given anatomical site, these so-called tissue  $T_{reg}$  cells were also shown to exhibit specific functional features to maintain corresponding organismal homeostasis. For example, during lung and muscle damages or ischemic stroke-induced brain injuries,  $T_{reg}$  cells in those respective tissues are able to secrete amphiregulin, a ligand of the epidermal growth factor receptor, to facilitate tissue repair<sup>4-6</sup>. Moreover, in the adipose tissue, adenosine generated by  $CD73^+$   $T_{reg}$  cells was recently reported to promote adaptive thermogenesis by activating beige fat biogenesis<sup>7</sup>. These studies have provided experimental evidence demonstrating the effector mechanisms underlying the nonimmunological role of  $T_{reg}$  cells in maintaining tissue homeostasis. However, like the aforementioned helper T cell-specific  $T_{reg}$  cells, how each tissue  $T_{reg}$  cell population controls its corresponding local immune responses remains poorly characterized.

To date, only a handful of suppressor molecules have been implicated in tissue  $T_{reg}$  cell-mediated immune regulation<sup>3</sup>, the most well characterized of which is IL-10. Yet mice with IL-10 deleted specifically in  $T_{reg}$  cells exhibited inflammation at multiple mucosal sites, indicating that IL-10, albeit not a universal  $T_{reg}$  cell suppressor molecule,

was still commonly utilized by different tissue  $T_{reg}$  cell subsets<sup>8</sup>. In addition,  $T_{reg}$  cell-derived IL-10 also does not seem to regulate a specific type of immune response because mice harboring  $T_{reg}$  cells incapable of producing IL-10 exhibited exacerbated  $T_H1$ ,  $T_H2$  and  $T_H17$  cell-driven tissue pathology<sup>8,9</sup>. By employing an experimental system that permits simultaneous examination of multiple tissue  $T_{reg}$  cell subsets during systemic autoimmunity, in the present study we identified distinct transcriptomic signatures in two different tissue  $T_{reg}$  cell populations that could account for their respective control of local inflammation. In particular, we found that IL-27, a pluripotent cytokine recognized for its regulatory properties<sup>10</sup>, is specifically induced in gut  $T_{reg}$  cells under inflammatory conditions. Moreover, IL-27 derived from  $T_{reg}$  cells, but not from other known intestinal IL-27-producing cell populations, is selectively needed for controlling  $T_H17$  cell responses in the gut-associated tissue. Loss of IL-27 expression by  $T_{reg}$  cells led to exacerbated  $T_H17$  cell-driven intestinal inflammation and colitis-associated cancer. Conversely, enhanced  $T_H17$  cell responses in mice with  $T_{reg}$  cell-specific IL-27 ablation could also help protect against enteric bacterial infection. Finally, single-cell transcriptomic analysis of intestinal  $T_{reg}$  cells revealed a distinct  $CD83^+CD62L^lo$   $T_{reg}$  cell subset that does not express IL-10 but is responsible for IL-27 production, particularly during intestinal inflammation. Together, our study uncovers a previously uncharacterized  $T_{reg}$  cell suppression mechanism that is pivotal to controlling a specific type of immune response in a particular tissue and provides further mechanistic insights into tissue-specific,  $T_{reg}$  cell-mediated immune regulation.

## Results

### Unique signatures in tissue $T_{reg}$ cells under inflammation

It has become evident that, like  $T_{conv}$  cells,  $T_{reg}$  cells differentiate into effector  $T_{reg}$  cells on activation and that both T cell receptor activation and cytokine stimulation play critical roles in inducing  $T_{reg}$  cell suppressor activity<sup>11,12</sup>. To capture the dynamic gene expression profiles in tissue  $T_{reg}$  cells involved in restricting ongoing inflammation in vivo, we employed an experimental system allowing us to simultaneously assess multiple tissue  $T_{reg}$  cells when they are actively controlling ongoing autoimmunity. In brief, multiorgan autoimmune inflammation was induced by  $T_{reg}$  cell ablation on diphtheria toxin (DT) administration in mice containing  $T_{reg}$  cells expressing the DT receptor (DTR) (*Foxp3<sup>DTR</sup>*)<sup>13</sup> (Extended Data Fig. 1a). The fatal consequence of DT-mediated  $T_{reg}$  cell ablation was then rescued via the transfer of congenically marked  $T_{reg}$  cells (Extended Data Fig. 1b,c). In this way, synchronized, in vivo, activated  $T_{reg}$  cells could be obtained without the contamination of recent thymic  $T_{reg}$  cell emigrants that have not been properly stimulated. Next,  $T_{reg}$  cells and  $T_{conv}$  cells from spleen as well as lung and small intestinal lamina propria (SI LP) were isolated from DT-treated *Foxp3<sup>DTR</sup>* mice or control phosphate-buffered saline (PBS)-treated mice 10 d after  $T_{reg}$  cell transfer for RNA-sequencing (RNA-seq) and comparative bio-informatics analysis. Although the DT-treated *Foxp3<sup>DTR</sup>* mice would eventually recover owing to the presence of transferred  $T_{reg}$  cells, at this time point,  $T_{conv}$  cells remained highly activated and expressed genes characteristic of  $T_H1$ ,  $T_H2$  and  $T_H17$  cell subsets of effector T ( $T_{eff}$ ) cells (Extended Data Fig. 1d).

Consistent with previous studies<sup>3</sup>, we found genes that are known to be upregulated in T<sub>reg</sub> cells from the nonlymphoid tissues, including transcription factors (for example, *Irf4*, *Nfil3*, *Id2*, *Rorc* and *Fosl2*), cytokine receptors (for example, *Il1rl1*), effector molecules (for example, *Il10*, *Klrg1*, *Areg*, *Gzmb*, *Fgl2*, *Metrn1* and *Lrb4r1*) and co-inhibitory molecules (for example, *Pdcd1* and *Lag3*), which were expressed at higher levels in T<sub>reg</sub> cells from lung and gut compared with those from spleen. Similarly, we also detected genes that are known to be expressed at the lower level in tissue T<sub>reg</sub> cells, such as *Id3*, *Tcf7*, *Bach2* and *Nrp1*, which were downregulated in T<sub>reg</sub> cells from lung and gut compared with those from spleen (Extended Data Fig. 1e). Nevertheless, despite a clear difference in gene expression observed in different tissue T<sub>reg</sub> cells subsets from either DT-treated *Foxp3<sup>DTR</sup>* mice or PBS-treated mice, as shown in the heatmap analysis (Extended Data Fig. 1f), the impact of inflammation on the transcriptional profiles in T<sub>reg</sub> cells (and T<sub>conv</sub> cells) was apparent. Consistently, principal component analysis (PCA) of RNA-seq results revealed a high degree of resemblance in T<sub>reg</sub> cells and T<sub>conv</sub> cells isolated from mice with DT treatment compared with the PBS-treated controls regardless of tissue origins (Extended Data Fig. 1g, top). On the other hand, both T<sub>reg</sub> cells and T<sub>conv</sub> cells in the same tissue also shared a considerable level of similarity in gene expression regardless of the presence or absence of inflammation (Extended Data Fig. 1g, bottom).

Next, we used scatter plots to compare genes that were differentially expressed in T<sub>reg</sub> cells versus T<sub>conv</sub> cells isolated from a particular tissue in mice with or without DT treatment (Fig. 1a–c). Only genes that are upregulated (red) or downregulated (blue) in T<sub>reg</sub> cells, when compared with T<sub>conv</sub> cells under the DT-treated condition, by more than 1.5-fold and at least 1.5-fold higher or lower than those under the PBS-treated condition, respectively, were considered to be potentially involved in T<sub>reg</sub> cell-mediated control of inflammation. Moreover, through Venn diagrams, we further identified genes that are commonly regulated in all or several T<sub>reg</sub> cell populations versus ones that are uniquely up- or downregulated in a given T<sub>reg</sub> cell subset over their T<sub>conv</sub> cell counterpart from a particular anatomical location during autoimmunity (Fig. 1d,e). Finally, gene ontology (GO) term enrichment analysis of differentially expressed genes (DEGs) in T<sub>reg</sub> cells from different tissues under DT-treated conditions revealed biological pathways that could be potentially critical for tissue T<sub>reg</sub> cell-mediated control of inflammation in a given tissue microenvironment (Fig. 1f,g). To this end, genes related to leukocyte proliferation could be observed in all T<sub>reg</sub> cell populations whereas genes related to regulation of T cell activation were specifically enriched in gut T<sub>reg</sub> cells (Fig. 1f). These results suggested that, although transferred T<sub>reg</sub> cells were all undergoing rapid expansion to control inflammation, regulation of T cell activation in the intestine required a specialized suppressor program employed by gut T<sub>reg</sub> cells.

### Specific IL-27 induction in gut T<sub>reg</sub> cells under inflammation

To gain further insight into the precise mechanisms by which tissue T<sub>reg</sub> cells control their corresponding local immune responses, we explored the identified tissue T<sub>reg</sub> cell-specific genes with a focus on the ones that have been previously associated with a role in immune regulation. Among the genes selectively upregulated in gut T<sub>reg</sub> cells from mice with ongoing inflammation (Fig. 1d, top), *Il27*, which encodes a subunit (IL-27p28) of a heterodimeric cytokine, IL-27, is of particular interest (Fig. 2a). IL-27, composed of EBI3

and IL-27p28, is a member of the IL-6/IL-12 superfamily. Previously, it was reported that IL-27 can directly inhibit the development of T<sub>H</sub>17 cells<sup>14,15</sup>. Moreover, IL-27 has also been shown to exert its suppressive effects indirectly through inducing IL-10 production by many T cell subsets or via promoting a specific T-bet<sup>+</sup>Foxp3<sup>+</sup> T<sub>reg</sub> cell population specialized to limit T<sub>H</sub>1 cell immunity<sup>16,17</sup>. However, even though T<sub>reg</sub> cells are known to express high levels of EBI3 (ref. 18), a finding that is also supported by our RNA-seq studies (Fig. 2b), it was IL-35, another heterodimeric cytokine composed of EBI3 and IL-12 $\alpha$  rather than IL-27p28, that has been previously shown to serve as a T<sub>reg</sub> cell suppressor molecule<sup>18</sup>. Nevertheless, in our RNA-seq studies and quantitative (q)PCR analysis, unlike *Il27* and *Ebi3*, the level of *Il12a* expression in T<sub>reg</sub> cells remained low irrespective of tissue origins or inflammatory conditions (Fig. 2c–f). Finally, we have also selectively detected a significantly increased amount of IL-27 protein but not IL-35 protein produced by intestinal T<sub>reg</sub> cells from mice treated with DT (Fig. 2g,h).

Notably, transferred T<sub>reg</sub> cells in DT-treated *Foxp3<sup>DTR</sup>* mice not only experienced autoimmune inflammation but were also under the pressure of filling up the niche in the absence of endogenous T<sub>reg</sub> cells. Therefore, we sought to determine whether elevated expression of IL-27 in intestinal T<sub>reg</sub> cells could also be observed in a different inflammatory setting. To this end, we employed an anti-CD3 monoclonal antibody-induced intestinal disease model in which treatment of anti-CD3 monoclonal antibody has been shown to lead to acute inflammation and intestinal pathology<sup>19</sup>. As shown in Fig. 2i–k, significantly increased expressions of both the transcript and protein of IL-27 were detected in gut T<sub>reg</sub> cells in mice receiving anti-CD3 monoclonal antibody treatment. These results suggested that elevated secretion of IL-27 by gut T<sub>reg</sub> cells is probably a common phenotype that could be detected in various inflammatory settings. It is interesting that such increases in IL-27 expression were greatly diminished in germ-free (GF) mice when compared with specific pathogen-free (SPF) counterparts, implying that, other than inflammation, commensal bacteria also play an important role in inducing IL-27 in gut T<sub>reg</sub> cells (Fig. 2i–k). It is noteworthy that elevated production of IL-10 by gut T<sub>reg</sub> cells was also detected (Extended Data Fig. 2). However, unlike IL-27, high levels of IL-10 expression in gut T<sub>reg</sub> cells could already be observed at steady state but with no clear further upregulation in the presence of inflammation. Collectively, our results suggested that, although T<sub>reg</sub> cell-derived IL-10 has been long recognized for its role in maintaining gut homeostasis<sup>8</sup>, IL-27 produced by T<sub>reg</sub> cells might play a more active role in controlling ongoing intestinal inflammation.

### T<sub>reg</sub> cell-derived IL-27 controls gut T<sub>H</sub>17 cell responses

To examine the function of IL-27 in T<sub>reg</sub> cell-mediated immune regulation, particularly in the intestine, we generated mice with T<sub>reg</sub> cell-specific deletion of IL-27p28 (*Foxp3<sup>Cre</sup>Il27<sup>fl/fl</sup>*). *Foxp3<sup>Cre</sup>Il27<sup>fl/fl</sup>* mice did not develop any obvious immune phenotype or autoimmune pathology (Fig. 3 and Extended Data Fig. 3). The frequencies and numbers of T<sub>reg</sub> cells in both lymphoid and nonlymphoid tissues were comparable between *Foxp3<sup>Cre</sup>Il27<sup>fl/fl</sup>* mice and their control littermates (Fig. 3a and Extended Data Fig. 3a,b). The suppression capacity of T<sub>reg</sub> cells isolated from the intestinal tissue was also not impeded by the absence of IL-27 production (Fig. 3b,c). Consequently, T<sub>conv</sub> cells remained under control because no difference in their proliferation and activation in *Foxp3<sup>Cre</sup>Il27<sup>fl/fl</sup>* mice could be

observed (Fig. 3d,e and Extended Data Fig. 3a,b). It is interesting that, despite exhibiting no detectable inflammatory responses, loss of IL-27 in T<sub>reg</sub> cells already resulted in a selective increase in the production of IL-17 by gut T<sub>eff</sub> cells without any immunological challenges (Fig. 3f,g and Extended Data Fig. 3b). Moreover, dysregulated IL-17 responses in *Foxp3<sup>Cre</sup>IL27<sup>fl/fl</sup>* mice were observed only in the gut because no alteration in T<sub>H</sub>17 cells was found elsewhere (Extended Data Fig. 3a). Finally, consistent with increased IL-17<sup>+</sup> T<sub>conv</sub> cells, *Foxp3<sup>Cre</sup>IL27<sup>fl/fl</sup>* mice also exhibited elevated frequencies of RORγt<sup>+</sup> T<sub>conv</sub> cells selectively in the intestine (Extended Data Fig. 3c,d). Notably, the percentage of IL-17<sup>+</sup> cells within the RORγt<sup>+</sup> T<sub>conv</sub> population was comparable in mice with or without T<sub>reg</sub> cell-specific IL-27 ablation (Extended Data Fig. 3e), a finding agreeing with the reported role of IL-27 in inhibiting T<sub>H</sub>17 cell differentiation rather than suppressing IL-17 expression<sup>15</sup>,

Previously, IL-27 was shown to directly act on T cells to suppress T<sub>H</sub>17 cell differentiation in a STAT1-dependent manner<sup>15</sup>. Consistently, we were also able to confirm a direct inhibitory effect of IL-27 on T<sub>H</sub>17 cells whereas interferon (IFN)-γ expression by T<sub>H</sub>1 cells was not impacted (Extended Data Fig. 4a,b). Moreover, it is also unlikely that T<sub>reg</sub> cell-derived IL-27 controls T<sub>H</sub>17 cell differentiation through impacting dendritic cell (DC) function because comparable expressions of cytokines known to drive T<sub>H</sub>17 cell differentiation were found in DCs from the gut of mice with or without T<sub>reg</sub> cell-specific IL-27 ablation (Extended Data Fig. 4c–h). Finally, mice with T cell-specific IL-27 receptor deletion (*CD4<sup>Cre</sup>IL27ra<sup>fl/fl</sup>*) exhibited elevated T<sub>H</sub>17 cell responses similar to those observed in *Foxp3<sup>Cre</sup>IL27<sup>fl/fl</sup>* mice (Extended Data Fig. 5). Together, these results strongly suggest that T<sub>reg</sub> cell-derived IL-27 regulates T<sub>H</sub>17 cell immunity primarily through directly targeting T cells.

It should also be noted, however, that DCs and other myeloid cells, as well as intestinal epithelial cells (IECs), have all been recently shown to regulate intestinal homeostasis through the production of IL-27 (ref. 20). To exclude the possibility that IL-27 secreted by different gut-resident cells could also contribute to the regulation of intestinal T<sub>H</sub>17 cell immunity, mice with DC- (*CD11c<sup>Cre</sup>IL27<sup>fl/fl</sup>*), myeloid cell- (*LysM<sup>Cre</sup>IL27<sup>fl/fl</sup>*) and IEC (*Vil1<sup>Cre</sup>IL27<sup>fl/fl</sup>*)-specific deletion of IL-27p28 were examined. As shown in Extended Data Fig. 5b–e, unlike *Foxp3<sup>Cre</sup>IL27<sup>fl/fl</sup>* and *CD4<sup>Cre</sup>IL27ra<sup>fl/fl</sup>* mice, we did not observe any alteration in T<sub>H</sub>17 cell frequencies in the aforementioned mouse lines compared with their corresponding littermate controls. Finally, to further confirm that the observed T<sub>H</sub>17 cell phenotype in *Foxp3<sup>Cre</sup>IL27<sup>fl/fl</sup>* mice is indeed due to the specific loss of T<sub>reg</sub> cell-derived IL-27, we performed the adoptive transfer study in which IL-27-deficient T<sub>reg</sub> cells were co-transferred with congenically marked Foxp3<sup>+</sup>CD4<sup>+</sup> T cells from *Foxp3<sup>KO</sup>* mice into RAG-deficient mice. Consistent with what we found in *Foxp3<sup>Cre</sup>IL27<sup>fl/fl</sup>* mice, IL-27-deficient T<sub>reg</sub> cells also selectively failed to restrain T<sub>H</sub>17 cells in the gut under this setting (Fig. 3h,i and Extended Data Fig. 3f), further supporting a nonredundant role of T<sub>reg</sub> cell-derived IL-27 in fine-tuning intestinal T<sub>H</sub>17 cell responses.

### Loss of T<sub>reg</sub> cell-derived IL-27 led to exacerbated gut diseases

As *IL27* is specifically upregulated in gut T<sub>reg</sub> cells under inflammation, we hypothesized that deletion of IL-27 in T<sub>reg</sub> cells would lead to an even stronger IL-17 response and



cause more severe intestinal immunopathology in disease settings. To this end, we employed the aforementioned anti-CD3 monoclonal antibody-driven intestinal disease model in which proinflammatory T<sub>H</sub>17 cells are predominantly responsible for the development of intestinal pathology<sup>21</sup>. Consistent with the aforementioned results from qPCR analysis, we could also detect significantly increased IL-27, but not IL-35, protein secretion by gut T<sub>reg</sub> cells from anti-CD3 monoclonal antibody-treated mice and the production of IL-27 was completely abolished in *Foxp3<sup>Cre</sup>IL27<sup>fl/fl</sup>* mice (Extended Data Fig. 6a,b). Moreover, as shown in Fig. 4a–c, we found that *Foxp3<sup>Cre</sup>IL27<sup>fl/fl</sup>* mice exhibited more pronounced weight loss along with more severe gut pathology compared with wild-type (WT) controls. The exacerbated disease phenotype was not due to insufficient T<sub>reg</sub> cell numbers because T<sub>reg</sub> cells from both *Foxp3<sup>Cre</sup>IL27<sup>fl/fl</sup>* mice and control littermates expanded to a similar degree in the attempt to control gut inflammation (Fig. 4d). Nevertheless, consistent with what we observed during homeostasis, only markedly increased IL-17 but not IFN- $\gamma$  responses were detected in *Foxp3<sup>Cre</sup>IL27<sup>fl/fl</sup>* mice (Fig. 4e,f). Similar results were also obtained from mice harboring T cells unresponsive to IL-27 whereas comparable T<sub>H</sub>17 cell responses were observed across mice with DC-, myeloid cell- and IEC-specific deletion of IL-27 and their corresponding WT controls on anti-CD3 monoclonal antibody administration (Extended Data Fig. 5f–j).

Previously, elevated T<sub>H</sub>17 cell responses were also shown to promote tumorigenesis in an azoxymethane (AOM)/dextran sulfate sodium (DSS) model of carcinogen-induced colitis-associated cancer (CAC)<sup>22</sup>. It is interesting that, during CAC tumorigenesis, it has been suggested that T<sub>reg</sub> cells could exhibit either anti- or protumor function depending on the timing during tumor development<sup>23</sup>. To this end, transient deletion of T<sub>reg</sub> cells during the early phase of CAC was shown to exacerbate intestinal inflammation that could promote tumorigenesis. It is thus plausible that loss of T<sub>reg</sub> cell-derived, IL-27-mediated regulation of gut T<sub>H</sub>17 cell responses could create a microenvironment favorable for tumor growth. Indeed, increased colon tumor burdens accompanied by significantly higher scores for inflammation ulceration and crypt distortion by histopathological analysis were observed in *Foxp3<sup>Cre</sup>IL27<sup>fl/fl</sup>* mice after the AOM and DSS treatment (Fig. 4g–i). Finally, selective increases in the frequencies of T<sub>H</sub>17 cells but not IFN- $\gamma$ -producing T<sub>H</sub>1 cells could be found in both large intestine (LI) and tumors in mice harboring T<sub>reg</sub> cells incapable of producing IL-27 (Fig. 4j,k). Together, by using both acute and chronic T<sub>H</sub>17 cell-driven intestinal inflammatory disease models, our results demonstrate a critical role of T<sub>reg</sub> cell-derived IL-27 in limiting gut pathology.

### T<sub>reg</sub> cell-derived IL-27 is dispensable to control EAE

Although T<sub>reg</sub> cell-derived IL-27 does not seem to play a noticeable role in tissues other than gut at steady state, it remains probable that IL-27 produced by T<sub>reg</sub> cells might still be required to control T<sub>H</sub>17 cell responses outside of the intestinal tissues when T<sub>H</sub>17 cell-driven inflammatory responses are triggered. To test this possibility, a central nervous system (CNS) autoimmune disorder, experimental autoimmune encephalomyelitis (EAE), in which autoreactive T<sub>H</sub>17 cells serve as central mediators in promoting disease pathogenesis, was employed<sup>24</sup>. Previously, IL-27 has been reported to limit neuroinflammation during EAE through directly suppressing the development of T<sub>H</sub>17 cells<sup>14</sup>. Consistently, mice with T cells incapable of responding to IL-27 harbored elevated frequencies of IL-17<sup>+</sup>

but not IFN- $\gamma$ <sup>+</sup> T<sub>eff</sub> cells in the CNS and exhibited a significant worsening of EAE (Fig. 5a–c). In contrast, no alteration in the frequencies of T<sub>H</sub>17 cells could be found in *Foxp3<sup>Cre</sup>IL27<sup>fl/fl</sup>* mice on EAE induction (Fig. 5d,e). Consequently, both *Foxp3<sup>Cre</sup>IL27<sup>fl/fl</sup>* mice and control littermates exhibited similar disease phenotypes (Fig. 5f). Altogether, although we confirmed a T cell-intrinsic role of IL-27 signaling in restricting T<sub>H</sub>17 cell responses in the CNS, unlike what was observed in the intestine, T<sub>reg</sub> cell-derived IL-27 is dispensable for controlling T<sub>H</sub>17 cell-driven neuroinflammation.

### ***Foxp3<sup>Cre</sup>IL27<sup>fl/fl</sup>* mice exhibited enhanced T<sub>H</sub>17 cell immunity**

Although uncontrolled T<sub>H</sub>17 cell responses have been frequently associated with intestinal immunopathology, they are also crucial for providing protection against many different pathogens at the mucosal surface<sup>25</sup>. Previously, it was shown that *Citrobacter rodentium*, a mouse pathogen that preferentially impacts the colon, can induce a strong local T<sub>H</sub>17 cell response that is necessary for protection<sup>26</sup>. Similar to the aforementioned autoimmune-driven inflammation models, we could also detect a substantial amount of IL-27 but not IL-35 secreted by T<sub>reg</sub> cells from the colon of *C. rodentium*-infected mice, whereas only minimal IL-27 production by T<sub>reg</sub> cells from the spleen could be observed (Extended Data Fig. 6c,d). It should be noted that, in agreement with a previous report<sup>27</sup>, during infection T<sub>conv</sub> cells were also capable of producing IL-27 (Extended Data Fig. 6c,d). Nevertheless, the amount of IL-27 secreted by gut T<sub>reg</sub> cells was still much higher compared with that by T<sub>conv</sub> cells (Extended Data Fig. 6d).

Next, we sought to determine the effect of T<sub>reg</sub> cell-specific IL-27 ablation on host defense against this enteric pathogen. As shown in Fig. 6a,b, we also found that *C. rodentium*-infected *Foxp3<sup>Cre</sup>IL27<sup>fl/fl</sup>* mice harbored elevated frequencies of IL-17<sup>+</sup> but not IFN- $\gamma$ <sup>+</sup> T<sub>eff</sub> cells in the colon. Consequently, significantly reduced bacterial burden in *Foxp3<sup>Cre</sup>IL27<sup>fl/fl</sup>* mice over littermate controls was observed (Fig. 6c), supporting our hypothesis that T<sub>reg</sub> cell-derived IL-27 regulates intestinal T<sub>H</sub>17 cell immunity. Nevertheless, it remains uncertain whether IL-27 produced by T<sub>reg</sub> cells would have a similar impact on the host defense against other enteric pathogens when a different type of immune response is triggered. To address this issue, we employed a *Toxoplasma gondii* infection model in which a strong IFN- $\gamma$ -mediated T<sub>H</sub>1 cell response is induced in the gut necessary for the clearance of this pathogen<sup>28</sup>. To this end, although increased frequencies of T<sub>H</sub>17 cells could still be observed in *Foxp3<sup>Cre</sup>IL27<sup>fl/fl</sup>* mice during *T. gondii* infection, comparable T<sub>H</sub>1 cell responses were elicited (Fig. 6d,e). Moreover, both *Foxp3<sup>Cre</sup>IL27<sup>fl/fl</sup>* mice and control littermates were able to control this parasitic pathogen efficiently (Fig. 6f). Collectively, our results from two different enteric pathogen models further demonstrate a selective regulatory effect of T<sub>reg</sub> cell-derived IL-27 on T<sub>H</sub>17 cell, but not T<sub>H</sub>1 cell, immunity, during intestinal infection.

### **IL-27 produced by a distinct gut T<sub>reg</sub> cell subset**

As several intestinal T<sub>reg</sub> cell populations have been reported to maintain gut homeostasis and intestinal tolerance<sup>29</sup>, it remains unclear whether IL-27 can be induced in the entire intestinal T<sub>reg</sub> cell population or there is a specific T<sub>reg</sub> cell subset primarily responsible for IL-27 production. To address this question, we performed single-cell RNA-seq (scRNA-seq) analysis of gut T<sub>reg</sub> cells from mice with or without *C. rodentium* infection. By



using dimensional reduction by uniform manifold approximation and projection (UMAP) for visualization of gut T<sub>reg</sub> cells, we observed four distinct T<sub>reg</sub> cell clusters (R0–R3) (Fig. 7a). T<sub>reg</sub> cells from the R0 cluster exhibit high expression of *Tcf7* but not *Sell*, resembling the previously reported activated T<sub>reg</sub> cells (Fig. 7b)<sup>30</sup>. On the other hand, the R1 cluster exhibits high expression of genes resembling effector T<sub>reg</sub> cells (for example, *Ill10* and *Gzmb*), whereas the R2 cluster expresses transcripts (for example, *Sell* and *Bach2*) indicative of resting T<sub>reg</sub> cells (Fig. 7b and Extended Data Fig. 7a,b)<sup>31,32</sup>. Finally, the R3 cluster is enriched with *Il1rl1* (that is, *St2*)-expressing cells (Fig. 7b and Extended Data Fig. 7c). It is interesting that, although the distribution of these four clusters was rather comparable between controls and *C. rodentium*-infected mice (Fig. 7c), *Il27* transcripts could be detected only in the R0 cluster from the infected group (Fig. 7d). Unfortunately, owing to the inherent lack of sensitivity of scRNA-seq for low-abundance transcripts such as cytokines<sup>33</sup>, only a few *Il27* transcript signals were detected. Nevertheless, we do not think that this is merely an experimental artifact because the signals of *Ebi3*, a gene that has been well recognized as being highly expressed in T<sub>reg</sub> cells, were also barely detectable (Fig. 7e). Unlike *Il27*, signals of *Ebi3* could be found in both R0 and R1 clusters, suggesting that the R0 cluster is enriched with IL-27-expressing T<sub>reg</sub> cells whereas the R1 cluster probably contains T<sub>reg</sub> cells that could produce other cytokines consisting of EBI3.

To further confirm our scRNA-seq results, we FACS analyzed intestinal T<sub>reg</sub> cell subsets from the infected mice based on the expressions of CD83 and transcription cell factor TCF1. CD83, a heavily glycosylated immunoglobulin-like, type 1 transmembrane protein, known to be a marker for activated T<sub>reg</sub> cell lineages<sup>34</sup>, was found to be one of the top ten highly expressed genes, along with *Tcf7* (the gene encoding TCF1) in the R0 cluster (Fig. 7b). Moreover, in addition to the R0 cluster, *Cd83* and *Tcf7* could also be detected in the R3 and R2 clusters to a lesser degree, respectively (Fig. 7f,g). As such, we could divide intestinal T<sub>reg</sub> cells into four clusters identified by our scRNA-seq analysis: R0: CD83<sup>+</sup>TCF1<sup>+</sup>; R1: CD83<sup>-</sup>TCF1<sup>-</sup>; R2: CD83<sup>-</sup>TCF1<sup>+</sup>; and R3: CD83<sup>+</sup>TCF1<sup>-</sup> (Fig. 7h). Next, we used CD62L (encoded by *Sell*) as a surrogate for TCF1 because it is also highly expressed in the R2 cluster (Fig. 7b and Extended Data Fig. 7b). Although we could not easily separate the R0 and R3 clusters, as both clusters are enriched with *Cd83<sup>-</sup>* but not *Sell*-expressing cells, three populations of T<sub>reg</sub> cells: R0 + R3 (CD83<sup>+</sup>CD62L<sup>lo</sup>; red), R1 (CD83<sup>-</sup>CD62L<sup>lo</sup>; green) and R2 (CD83<sup>-</sup>CD62L<sup>hi</sup>; blue) clusters were FACS isolated and subjected to qPCR (Fig. 7i). As shown in Fig. 7j,k, the R0 (and R3) cluster-enriched T<sub>reg</sub> cells expressed high levels of *Il27* and *Ebi3* whereas the R1 cluster-enriched T<sub>reg</sub> cells expressed only *Ebi3*. On the other hand, only the R1 cluster-enriched T<sub>reg</sub> cells expressed high levels of *Il10*, whereas none of these three genes was found to be highly expressed in the R2 cluster-enriched T<sub>reg</sub> cells, consistent with the aforementioned effector and resting T<sub>reg</sub> cell features in the R1 and R2 clusters, respectively (Fig. 7l). It should be noted that, even though CD83<sup>+</sup>CD62L<sup>lo</sup> T<sub>reg</sub> cells could also be found in the spleen, expression of *Il27* could not be detected, further supporting our previous findings of selective *Il27* induction in gut T<sub>reg</sub> cells. Finally, unlike *Cd83*, it seems that the previously identified intestinal T<sub>reg</sub> cell genes such as *Rorc* and *Gata3* could not be used to specifically mark these IL-27-expressing T<sub>reg</sub> cells (Extended Data Fig. 7d). Together, our studies identify a new CD83<sup>+</sup>CD62L<sup>lo</sup> T<sub>reg</sub> cell subset, which is distinct from other T<sub>reg</sub> cell populations previously reported in the intestine, responsible

for IL-27 production, and that IL-27-expressing T<sub>reg</sub> cells are pivotal in controlling intestinal T<sub>H</sub>17 cell immunity, particularly under inflammatory conditions.

## Discussion

As opposed to the original concept that T<sub>reg</sub> cells provide a generic level of immune regulation, it is now well appreciated that there is a high level of heterogeneity in T<sub>reg</sub> cell populations to effectively control a wide range of immune responses in different tissue microenvironments. Our studies have clearly demonstrated that, under different inflammatory conditions, IL-27 can be specifically induced in gut T<sub>reg</sub> cells, raising an important question as to what makes the intestinal microenvironment unique for IL-27 expression in T<sub>reg</sub> cells. It has been previously documented that the production of IL-27 by macrophages can be induced in a toll-like receptor (TLR)/MyD88-dependent manner<sup>35</sup>. Even though the expression of IL-27 has never been reported in T<sub>reg</sub> cells, MyD88-dependent sensing of gut microbiome by T<sub>reg</sub> cells has been shown to be critical in establishing intestinal tolerance and that T<sub>reg</sub> cells devoid of MyD88 exhibited a selective defect in controlling IL-17 responses in the gut mucosa<sup>36</sup>. Owing to a strong resemblance between the findings in mice with T<sub>reg</sub> cell-specific deletion of IL-27 and MyD88, it is intriguing to speculate that loss of IL-27 induction in MyD88-deficient T<sub>reg</sub> cells could be the underlying mechanism responsible for the dysregulated intestinal T<sub>H</sub>17 cell responses. Furthermore, dysbiotic gut microbiota, particularly under inflammatory conditions, also probably serve as important environmental factors to drive the expression of IL-27 in gut T<sub>reg</sub> cells, a notion that is directly supported by our analysis of GF animals on anti-CD3 monoclonal antibody treatment. Nevertheless, future studies employing whole-genomic sequencing and gnotobiotic approaches are required to identify specific microbes that functionally contribute to the induction of IL-27 in intestinal T<sub>reg</sub> cells.

Loss of IL-27 signaling has also been previously shown to lead to enhanced IFN- $\gamma$  responses<sup>37</sup>. Therefore, it seems puzzling why we did not see an effect on IFN- $\gamma$  responses when IL-27 production was ablated in T<sub>reg</sub> cells. Moreover, our study suggests that only IL-27 derived from T<sub>reg</sub> cells, but not from other known IL-27-producing cell populations, is responsible for regulating T<sub>H</sub>17 cell responses in the intestine. These results were also surprising because the IL-27-expressing T<sub>reg</sub> cells do not seem to be the major T<sub>reg</sub> cell subset in the intestine, as suggested by our scRNA-seq study, and the amount of IL-27 secreted by T<sub>reg</sub> cells is also not likely to be higher than that made by other IL-27 producers in the gut. However, these findings were not completely unexpected. First, although IL-27 is capable of limiting both T<sub>H</sub>1 and T<sub>H</sub>17 cell responses *in vivo*<sup>10</sup>, it does not seem to repress but might rather promote T<sub>H</sub>1 cell differentiation through the activation of STAT1 and the induction of T-bet (T-box transcription factor TBX21)<sup>38</sup>. Second, we have recently demonstrated that IL-27 secreted by DCs, other myeloid cells and IECs plays distinct roles in promoting intestinal homeostasis both at steady state and during infection<sup>20</sup>. Specifically, IL-27 produced by DCs was shown to be critical for the differentiation of T-bet<sup>+</sup> T<sub>reg</sub> cells, a specific T<sub>reg</sub> cell subset that is required to control IFN- $\gamma$ -mediated T<sub>H</sub>1 cell immunity<sup>39</sup>. These results, combined with the current work, suggested that, unlike its direct inhibitory effect on T<sub>H</sub>17 cells, IL-27 controls T<sub>H</sub>1 cell responses indirectly through the induction of T-bet<sup>+</sup> T<sub>reg</sub> cells. Our studies also further implied that different IL-27-producing cells and

their responding cells probably reside in close proximity and directly interact with each other to achieve such a selective effect. As such, the precise location in the intestinal tissue that the IL-27-producing T<sub>reg</sub> cells inhabit is also probably the place where T<sub>H</sub>17 cells differentiate: an intriguing hypothesis that warrants further investigation.

Previously, a specific subset of ROR $\gamma$ t-expressing intestinal T<sub>reg</sub> cells known to be important to maintain gut homeostasis was shown to be induced in the periphery in a gut microbiota-dependent manner<sup>40,41</sup>. It is interesting that, despite a similar reliance of microbiome on the induction of IL-27- and ROR $\gamma$ t-expressing T<sub>reg</sub> cells, our scRNA-seq analysis suggested that not all ROR $\gamma$ t<sup>+</sup> T<sub>reg</sub> cells could produce IL-27. It is possible that gut microbiota can drive the expression of IL-27 in a certain T<sub>reg</sub> cell population (that is, CD83<sup>+</sup>) within both gut-resident periphery-induced and thymus-derived T<sub>reg</sub> cells. Considering the diverse features of the intestinal microenvironment, one probably should not be surprised that gut T<sub>reg</sub> cells can exhibit many unique characteristics. The presence of these functionally distinct T<sub>reg</sub> cell subsets in the intestine further implies the presence of a certain division of labor between different gut T<sub>reg</sub> cell subsets to coordinately maintain intestinal homeostasis.

In humans, genome-wide association studies have identified IL-27 as a candidate gene within a susceptibility locus for inflammatory bowel disorder (IBD)<sup>42</sup>. Significantly, less IL-27 was found in people harboring the risk alleles relative to those with the nonrisk alleles<sup>43</sup>. These studies provided evidence linking IL-27 and IBD and suggested that the observed elevations in IL-27 in certain patients probably represent an anti-inflammatory response, albeit insufficient to control the ongoing intestinal inflammation<sup>42</sup>. Nevertheless, it should also be noted that there are reports pointing to a proinflammatory role of IL-27 in promoting colitis<sup>44,45</sup>. These seemingly contradictory findings further demonstrated the complex nature of this cytokine because IL-27 can exert its diverse activities depending on the cell type that produces it, the cell type that responds to it, as well as the location and probably the timing when the stimulation occurs. In the present study, our studies clearly show that T<sub>reg</sub> cell-derived IL-27 plays a dominant and nonredundant role in regulating intestinal T<sub>H</sub>17 cell responses. The approach taken in this work not only allowed us to identify IL-27 as a T<sub>reg</sub> cell suppressor molecule selectively required for controlling a particular type of immune response in a specific tissue location, but also established a powerful platform for future investigation into tissue-specific T<sub>reg</sub> cell suppressor programs.

## Methods

### Mice

Swiss Webster mice, CBA/CaJ mice, Ly5.1<sup>+</sup> *Foxp3*<sup>KO</sup> mice<sup>46</sup>, *Foxp3*<sup>DTR</sup> mice<sup>13</sup>, *Foxp3*<sup>Thy1.1</sup> mice<sup>47</sup>, *CD11c*<sup>Cre</sup> *Il27*<sup>fl/fl</sup> mice, *LysM*<sup>Cre</sup> *Il27*<sup>fl/fl</sup> mice, *Vil1*<sup>Cre</sup> *Il27*<sup>fl/fl</sup> mice and *CD4*<sup>Cre</sup> *Il27ra*<sup>fl/fl</sup> mice have been described previously<sup>20</sup>. T<sub>reg</sub> cell-specific deletion of IL-27p28 was achieved by breeding *Il27*<sup>fl/fl</sup> mice to *Foxp3*<sup>Cre</sup> mice (also expressing the Foxp3-driven yellow fluorescent protein (YFP) reporter)<sup>8</sup>. All mice were bred and housed under SPF conditions. GF animal studies were done in collaboration with H. Chu (University of California, San Diego) and those mice were housed in the dedicated GF facility equipped with flexible-film isolators. Mice aged 8 to ~12 weeks of both sexes were

used and only *Foxp3<sup>Cre</sup>* WT littermates of the same gender served as controls in each experiment. All mice were housed at a temperature between 18 °C and 23 °C with 40–60% humidity. A 12-h light:12-h dark cycle was used. Mice were maintained and handled in accordance with the Institutional Animal Care and Use Guidelines of the University of California, San Diego and National Institutes of Health (NIH) Guidelines for the Care and Use of Laboratory Animals and the Animal Research: Reporting In Vivo Experiments (ARRIVE) guidelines.

### Flow cytometry and antibodies

The antibodies were all used at a dilution of 1:400 unless specifically specified below. Cells were stained with Ghost Dye Red 780 (catalog no. 13-0865-T100, Tonbo Biosciences), followed by surface and intracellular antibody staining for CD4 (catalog no. 45-0042-82), Ki67 (catalog no. 51-5698-82), CD62L (catalog no. 12-0621-82), CD8 $\alpha$  (catalog no. 25-0081-82), CD44 (catalog no. 48-0441-80), IFN- $\gamma$  (catalog no. 25-7311-82), IL-17A (catalog no. 48-7177-82), ROR $\gamma$ t (catalog no. 61-6981-82), CD25 (catalog 12-1522-82), ST2 (catalog 46-9335-82) and Foxp3 (catalog no. 53-5773-82, 1:200 dilution for staining) (all from Thermo Fisher Scientific); and CD83 (catalog no. 121508, BioLegend) and TCF1 (catalog no. 6709S, Cell Signaling, 1:200 dilution for staining) at the manufacturers' recommended concentrations. Fixation and permeabilization of cells were performed with reagents from the Tonbo Biosciences FOXP3/Transcription Factor Staining Kit (catalog no. TNB-0607). To detect cytokine production, cells were stimulated in a 96-well plate with 50 ng ml<sup>-1</sup> of phorbol 12-myristate 13-acetate, 0.5  $\mu$ g ml<sup>-1</sup> of ionomycin, and 1  $\mu$ g ml<sup>-1</sup> of Brefeldin A (all from Sigma-Aldrich) in complete 5% Roswell Park Memorial Institute (RPMI) medium for 4 h at 37 °C before staining. An LSRFortessa or LSRFortessa X20 cell analyzer (BD Biosciences) was used for data collection and FACSDiva and FlowJo software (BD Biosciences) for data analysis.

### In vivo activation of T<sub>reg</sub> cells

To eliminate endogenous T<sub>reg</sub> cells, *Foxp3<sup>DTR</sup>* mice were injected with 50  $\mu$ g of DT per kg body weight or PBS intraperitoneally for 2 d consecutively and every other day thereafter as described previously<sup>13</sup>. On the second day of DT injection,  $2 \times 10^6$  CD4<sup>+</sup>Foxp3<sup>Thy1.1+</sup> T<sub>reg</sub> cells from the spleen and lymph nodes (LNs) of unmanipulated *Foxp3<sup>Thy1.1</sup>* mice were sorted by FACS and transferred into *Foxp3<sup>DTR</sup>* mice intravenously. CD4<sup>+</sup>Foxp3<sup>Thy1.1+</sup> T<sub>reg</sub> cell and CD4<sup>+</sup>Foxp3<sup>Thy1.1-</sup> T<sub>conv</sub> cell populations from different tissues (that is, spleen, lung and SI LP) of DT- and PBS-treated *Foxp3<sup>DTR</sup>* mice were respectively isolated 10 d after T<sub>reg</sub> cell transfer. All T cell populations were first enriched by positive selection with CD4 MojoSort beads (BioLegend) before FACS.

### Tissue preparation and cell isolation

Spleen and LNs were mechanically dissociated between frosted glass slides or with the back of a syringe plunger and filtered through a 100- $\mu$ m nylon mesh to yield single-cell suspensions. For isolation of lymphocytes from lung, SI LP, LI LP or tumor, after perfusion, tissues were harvested and minced before transferring to conical tubes. The minced pieces were resuspended in 10 ml of complete RPMI-1640 containing 1% penicillin–streptomycin, 20 mM HEPES, pH 7.4, 0.05 mg ml<sup>-1</sup> of Liberase TL (Roche) and 0.05% DNase I (Roche)

and shaken for 30 min at 37 °C in 50-ml Falcon tubes. The tissue suspension was collected and passed through a 70- $\mu$ m cell strainer and the cells were pelleted by centrifugation at 300g. The cells were then resuspended and purified by 47% Percoll and centrifuged at 400g for 10 min. The pellet was collected, washed and resuspended in complete RPMI medium.

### Gene expression profiling

Poly(A) RNA-seq was performed using three biological replicates for each sorted cell population. Reads were mapped to mouse genome v.mm9 with STAR aligner, counts were generated using htseq/0.6.1 and differential gene expression analysis was conducted using DESeq2/1.30.1 in R. DEGs in T<sub>reg</sub> cells compared with T<sub>conv</sub> cells from their respective tissue origin and treatment condition were generated in DESeq2 using negative binomial generalized linear model fitting with Wald's test for significance and the Benjamini–Hochberg correction for multiple testing. The DEGs with adjusted  $P > 0.05$  were plotted in scatter plots and used to create the Venn diagrams. Genes annotated as upregulated or downregulated in the scatter plots were used for GO analysis, which was conducted for biological processes using enrichGO in the clusterProfiler package with the following parameters: pvalueCutoff = 0.05, qvalueCutoff = 0.02, pAdjust-Method = Benjamini–Hochberg, dropGO level 5 and simplify cutoff 0.5. Count data were transformed using variance stabilizing transformation for visualization with heatmaps and PCA plots. Violin plots were created for specific genes using normalized counts from DESeq2.

For scRNA-seq analysis, CD45<sup>+</sup> immune cells isolated from the large intestine of uninfected mice and mice 10 d after *C. rodentium* infection were sent for single-cell library preparation according to the protocol for 10 $\times$  Genomics for Single Cell 5' Gene Expression. About 10,000 sorted CD45<sup>+</sup> cells were loaded and partitioned into Gel Bead In-Emulsions. The fastq files were aligned to the mm10 mouse genome using the Cell Ranger (v.7.0.0) pipeline, including intronic reads. The Seurat (v.4.1.0) package in R (v.4.1.2) was used for the gene expression analysis. Cells that were dying were first removed by filtering out cells with fewer than 200 genes or 500 transcripts or >10% mitochondrial content. All the cells captured were then clustered and the cluster that had the highest expression of Foxp3, as well as a transcriptomic signature of T<sub>reg</sub> cells, was selected for further analysis. This T<sub>reg</sub> cell subset included 242 cells from the infected group and 282 from the uninfected group. Differential gene expression analysis was done using the FindMarkers function within the Seurat package, which uses Wilcoxon's rank-sum test.

### Analysis by qPCR

For quantification of *Ii27*, *Ebi3*, *Ii12a* and *Ii10* expression, T<sub>conv</sub> cells and T<sub>reg</sub> cells in different tissues from DT- and PBS-treated *Foxp3<sup>DTR</sup>* mice or from *Foxp3<sup>Cre</sup>Ii27<sup>fl/fl</sup>* and WT littermates were sorted on a FACS Aria Fusion cell sorter (BD Biosciences) with a purity of >95%. For certain experiments, WT *Foxp3<sup>Cre</sup>* mice were infected with *C. rodentium* as described below. Then, 10 d after infection, splenocytes and colonic immune cells were extracted, followed by FACS isolation of CD83<sup>+</sup>CD62L<sup>lo</sup>, CD83<sup>-</sup>CD62L<sup>lo</sup> and CD83<sup>-</sup>CD62L<sup>hi</sup>CD4<sup>+</sup>Foxp3<sup>YFP+</sup> T<sub>reg</sub> cells. CD62L<sup>hi</sup> T<sub>reg</sub> cells were used as the reference for the CD83<sup>-</sup> population because CD62L and CD83 are not co-expressed in the same T<sub>reg</sub> cells based on our scRNA-seq analysis. For DC cytokine expression

profiling, CD11c<sup>+</sup> DCs from the spleen or SI of *Foxp3<sup>Cre</sup>Il27<sup>fl/fl</sup>* and WT littermates were sorted. Cells were stimulated with or without lipopolysaccharide (LPS; 1  $\mu\text{g ml}^{-1}$ ) for 6 h at 37 °C followed by RNA isolation using an RNeasy Kit (QIAGEN). Extracted RNA was converted to complementary DNA with an iScript cDNA Synthesis Kit (BioRad), followed by qPCR reactions using SYBR Select Master Mix (Thermo Fisher Scientific). All real-time reactions were run on a 7900HT Fast Real-Time PCR System (Thermo Fisher Scientific) with the following primers: *Il27*: 5'-CTGAATCTCGATTGCCAGGAGTGA-3' (forward) and 5'-AGCGAGGAAGCAGAGTCTCTCAGAG-3' (reverse); *Ebi3*: 5'-CGGTGCCCTACATGCTAAAT-3' (forward) and 5'-GCGGAGTCGGTACTTGAGAG-3' (reverse); *Il12a*: 5'-CAGGCTACCTC CTCTTTTTTG-3' (forward) and 5'-CAGCAGTGCAGGAATAATGTT-3' (reverse); *Il10*: 5'-CAGAGCCACATGCTCCTAGA-3' (forward) and 5'-TGTCCAGCTGGTCCTTTGTT-3' (reverse); *Il1b*: 5'-ACTCATTGT GGCTGTGGAGA-3' (forward) and 5'-TTGTTTCATCTCGGAGCCTGT-3' (reverse); *Il6*: 5'-TGAACAACGATGATGCACCTTG-3' (forward) and 5'-CTGAAGGACTCTGGCTTTGTC-3' (reverse); *Il23*: 5'-CCAGCGG GACATATGAATCT-3' (forward) and 5'-AGGCTCCCCTTTGAAGATGT-3' (reverse); *Tgfb*: 5'-GGAGAGCCCTGGATACCAAC-3' (forward) and 5'-AAGTTGGCATGGTAGCCCTT-3' (reverse); and *Il12b*: 5'-AGGT CACTGGACCAAAGG-3' (forward) and 5'-TGGTTTGTGATGATGTC CCTGA-3' (reverse).

## ELISA

For quantification of the production of IL-27, IL-35 and IL-10, T<sub>conv</sub> cells and T<sub>reg</sub> cells in different tissues from DT- and PBS-treated *Foxp3<sup>DTR</sup>* mice or from anti-CD3 monoclonal antibody-treated or *Citrobacter*-infected *Foxp3<sup>Cre</sup>Il27<sup>fl/fl</sup>* and WT littermates were sorted on a FACS Aria Fusion cell sorter with a purity of >95%. Cells were stimulated with LPS (0.5  $\mu\text{g ml}^{-1}$ ) for 48 or 72 h at 37 °C. Supernatant was collected and measured by ELISA kits according to the manufacturer's instructions (catalog nos. 438707, 440507 and 431414, BioLegend). Absorbance was measured at 450 nm with a microplate reader (Molecular Devices).

## In vitro suppression assay

Carboxyfluorescein diacetate succinimidyl ester (CFSE)-labeled, naive CD4<sup>+</sup>CD25<sup>-</sup>CD62L<sup>hi</sup> T cells,  $4 \times 10^4$ , from Ly5.1<sup>+</sup> B6 mice and CD4<sup>+</sup>Foxp3<sup>+</sup>YFP<sup>+</sup> T<sub>reg</sub> cells in SI LP or spleen from *Foxp3<sup>Cre</sup>Il27<sup>fl/fl</sup>* mice or WT control littermates were co-cultured in a 96-well U-bottomed plate at the indicated ratios and stimulated with 1  $\mu\text{g ml}^{-1}$  of anti-CD3 monoclonal antibody (catalog no. BE0001-1, Bio-X-Cell) in the presence of  $15 \times 10^4$  mitomycin C-treated, T cell-depleted splenocytes from B6 mice for 72 h at 37 °C. CFSE dilution was assessed by FACS analysis.

## In vitro IL-27 inhibition assay

Naive CD4<sup>+</sup>CD25<sup>-</sup>CD62L<sup>hi</sup> T cells,  $1 \times 10^6$ , from Ly5.1<sup>+</sup> B6 mice were cultured in a 24-well plate and stimulated with 1  $\mu\text{g ml}^{-1}$  of anti-CD3 monoclonal antibody in the presence of  $2 \times 10^6$  mitomycin C-treated, T cell-depleted splenocytes from B6 mice and 50 U ml<sup>-1</sup> of recombinant human IL-2 (PeproTech) under T<sub>H</sub>1 cell- or T<sub>H</sub>17 cell-polarizing



conditions for 4 d at 37 °C. The cell polarization medium was supplemented as follows: for T<sub>H</sub>1 cell differentiation, 2 U ml<sup>-1</sup> of IL-12 (PeproTech) and 10 µg ml<sup>-1</sup> of anti-IL-4 monoclonal antibody (catalog no. BE0045, Bio-X-Cell); for T<sub>H</sub>17 cell differentiation, 2 ng ml<sup>-1</sup> of human transforming growth factor (hTGF-β, PeproTech) and 20 ng ml<sup>-1</sup> of IL-6 (PeproTech). In some samples, 100 ng ml<sup>-1</sup> of IL-27 (BioLegend) was added. Surface and intracellular cytokines were stained and analyzed as previously described.

### Adoptive T cell transfer study

CD4<sup>+</sup> T cells,  $1.6 \times 10^6$ , isolated from spleen and LNs of Ly5.1<sup>+</sup> *Foxp3*<sup>KO</sup> mice, mixed with  $4 \times 10^5$  CD4<sup>+</sup>Foxp3<sup>YFP+</sup> T<sub>reg</sub> cells isolated from spleen and LNs of *Foxp3*<sup>Cre</sup>*Il27<sup>fl/fl</sup>* mice or their WT littermates, were intraperitoneally injected into *Rag1*<sup>-/-</sup> recipients. Mice were sacrificed 3 weeks after cell transfer or when mice reached <80% of their original body weight. Colonic immune cells were isolated for FACS analysis as described above.

### Anti-CD3 monoclonal antibody-induced intestinal inflammation

Anti-CD3 monoclonal antibodies were injected intraperitoneally 3× (20, 20 and 20 µg per mouse) every other day. On day 5, mice were taken down for histology, tissue preparation, cell isolation and immune staining.

### *T. gondii* Infection

The ME-49 strain of *T. gondii* was maintained in Swiss Webster and CBA/CaJ mice and tissue cysts from the brain were used for infection as previously described<sup>20</sup>. For all studies, mice were infected with 40 cysts of ME-49 by an oral route and analyzed for parasite burden. To quantify parasite burden, qPCR was performed for DNA isolated from duodenum and liver of infected mice using primers 5'-TCCCCTCTGCTGGCGAAAAGT-3' (forward) and 5'-AGCGTTCGTGGTCAACTATCGATTG-3' (reverse) to determine the relative abundance of *T. gondii* *B1* gene to mouse *Gapdh* gene. The PCR reaction was run using the standard setting on Applied Biosystems 7900 as described previously<sup>20</sup>.

### *C. rodentium* Infection

For infections, *C. rodentium* (DBS100 strain) was cultured overnight from a single colony in lysogeny broth (LB) with nalidixic acid (Nal) from day 1. On day 0, each mouse was infected with  $5.0 \times 10^9$  colony-forming units (c.f.u.) per mouse in a volume of 100 µl by oral gavage. On day 10, mice were taken down for tissue preparation, cell isolation and immune staining. To quantify bacterial burden, LI tissue samples were also collected and homogenized in LB medium at day 10 post-infection. The numbers of bacteria were counted by plating dilutions of the excess inocula sample on to LB agar with Nal as previously described<sup>48</sup>.

### AOM/DSS-induced, colitis-associated cancer

For induction of colon cancer, mice were intraperitoneally injected with 10 mg kg<sup>-1</sup> of AOM (Sigma-Aldrich). After 5 d, mice were supplied with 2% DSS solution for 5 d followed by normal drinking water for 15 d. The DSS cycle was repeated 3× and mice were taken down after the last DSS cycle for tissue preparation, cell isolation and immune

staining<sup>49</sup>. AOM-induced tumors will form in the colon. The tumor formation is painless and does not metastasize.

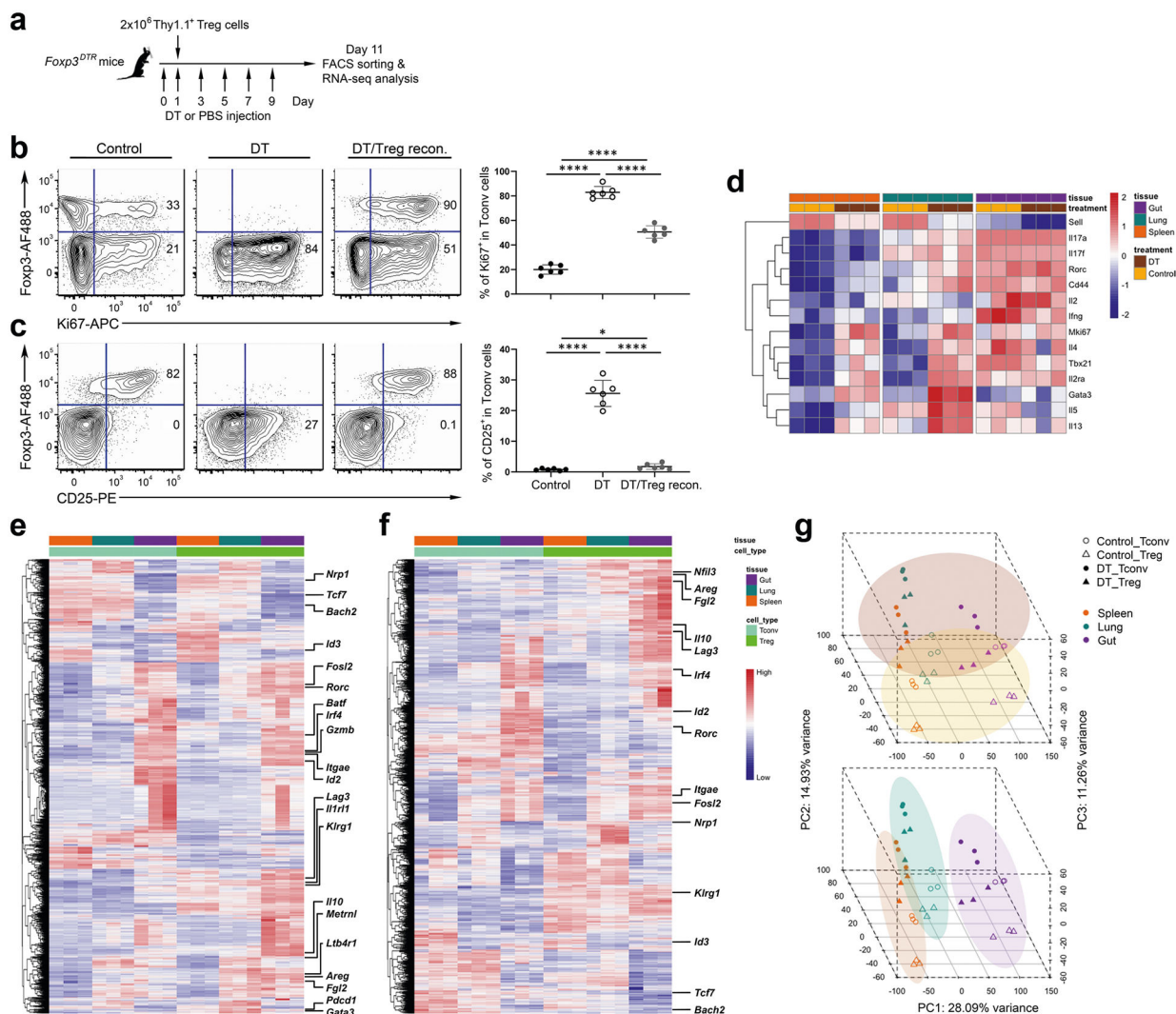
### Histology

To assess immunopathology, different tissues were harvested and immediately fixed in 10% formalin solution. Paraffin-embedded sections were cut (5-mm thickness) and stained with hematoxylin and eosin (H&E). All slides were digitized and imaged using the Olympus Nanozoomer and Digital Pathology viewing software (Nikon). Histopathology of SI in the anti-CD3 monoclonal antibody-induced, intestinal inflammation model and LI in the AOM/DSS-induced, colitis-associated cancer model was examined and blindly scored using the scale of 0–4 and 0–15, respectively, as previously described<sup>39,50</sup>.

### Statistics and reproducibility

Statistical analysis was applied to technical replicates or biologically independent mice for each experiment. All experiments described in the present study have been performed independently at least twice and the exact numbers of independent experiments with similar results are indicated in the figure captions. GraphPad Prism 8 software was used for data analysis and representation. *P* values for comparisons are provided as exact values or as  $P < 0.0001$ . The 95% confidence levels were used to determine statistically significant *P* values. No statistical methods were used to predetermine sample sizes, but our sample sizes were similar to those reported in previous publications. The data met the assumptions of the statistical tests used. Data distributions (individual data points) have been shown in all figures when applicable and were assumed to be normal, but this was not formally tested. Mice were sex and age matched and littermates were used whenever possible. Mice were then allocated into experimental groups according to their genotypes. Data collection and analysis were not performed blind to the conditions of the experiments, except for the H&E staining-based immunopathology analysis. No data points or animals were excluded from the analysis, except for mice that needed to be prematurely euthanized owing to a display of unrelieved clinical signs of pain or those that had lost >20% of their pre-procedure body weight based on our approved animal protocol.

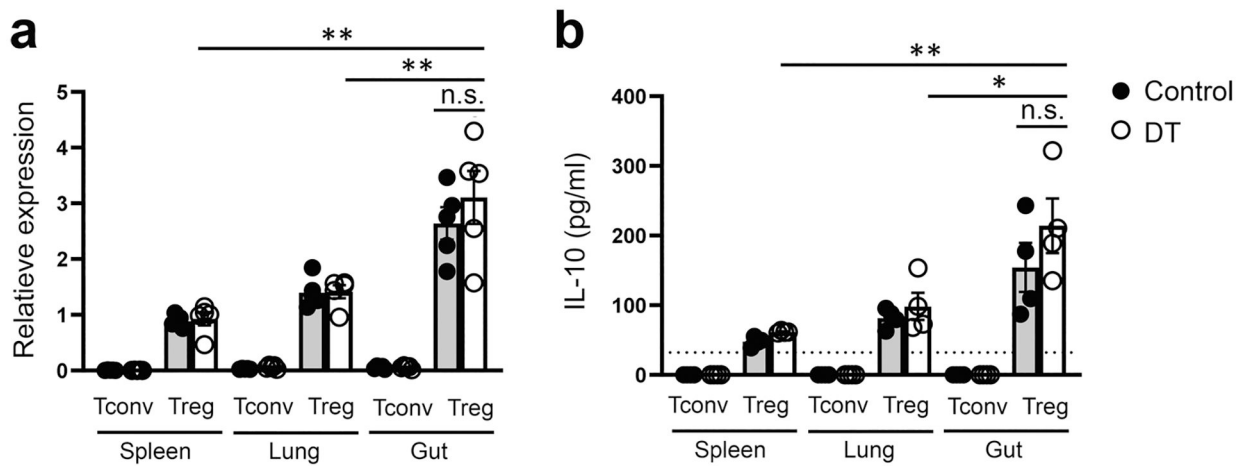
## Extended Data



**Extended Data Fig. 1 | Establishing an in vivo experimental model to simultaneously study active suppressor program in different tissue Treg cell subsets.**

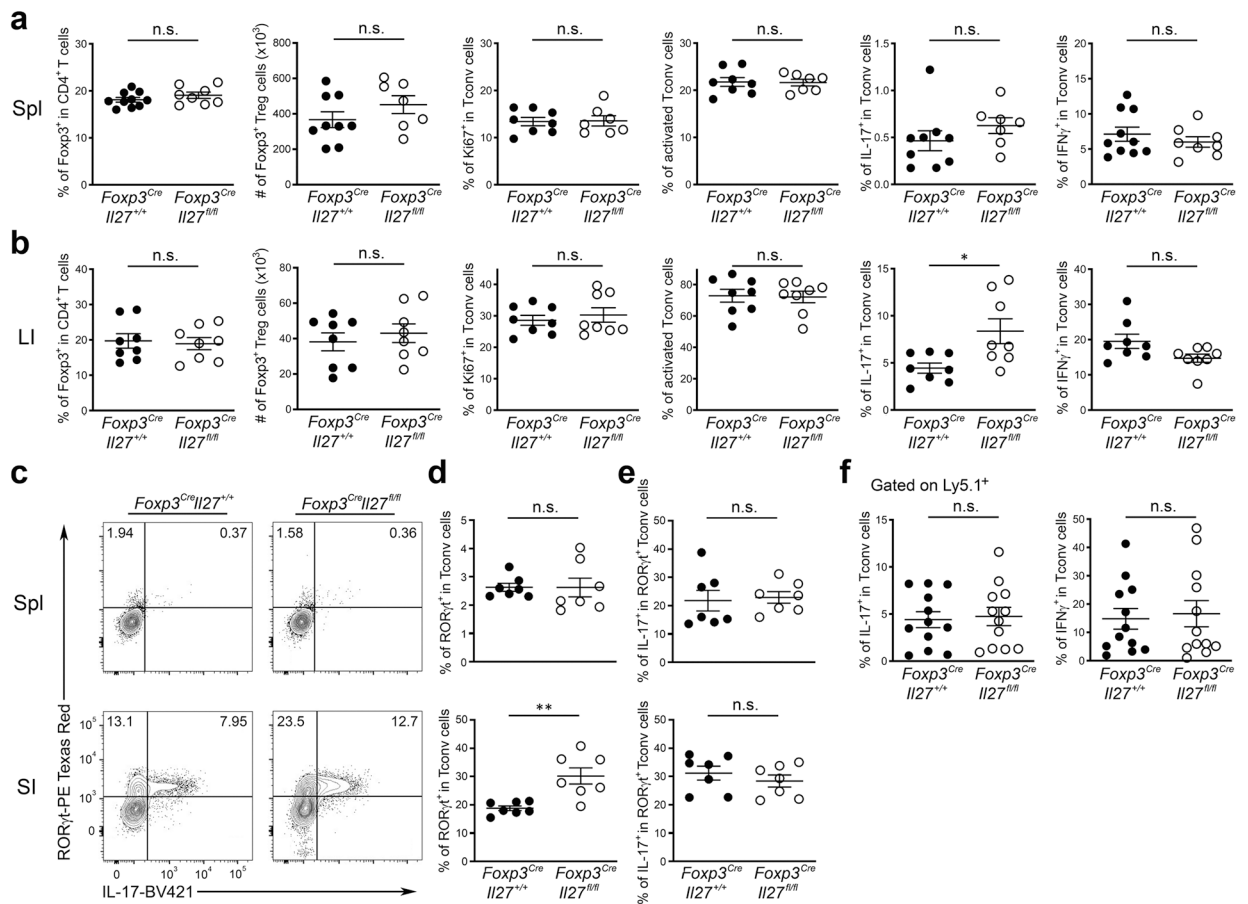
**a**, Schematic of the experimental model for studying Treg cell-mediated control of systemic autoimmunity. FACS analysis and frequencies of **b**,  $Ki67^+$  and **c**,  $CD25^+$  cells within the Tconv cells gated on the live  $CD4^+Foxp3^-$  population (or Treg cells gated on the live  $CD4^+Foxp3^+$  population) in spleens of control PBS-treated or DT-treated  $Foxp3^{DTR}$  mice with or without transfer of  $Foxp3^{Thy1.1+}$  Treg cells. Each symbol represents an individual mouse ( $n = 6$ ). Data are presented as mean values  $\pm$  SD. In **b**, \*\*\*\*  $P < 0.0001$  (up); \*\*\*\*  $P < 0.0001$  (bottom left); \*\*\*\*  $P < 0.0001$  (bottom right). In **c**, \*  $P = 0.0352$  (up); \*\*\*\*  $P < 0.0001$  (bottom left); \*\*\*\*  $P < 0.0001$  (bottom right). Statistical significance was determined by two-tailed unpaired t test. **d**, Heatmap of selected genes characteristic of activated T cells as well as Th1, Th2 and Th17 subsets that were expressed in Tconv cells isolated from indicated tissues in control PBS-treated or DT-treated  $Foxp3^{DTR}$  mice 10 days after Treg cell transfer. Heatmaps of top 10% of most variable genes in Treg cells isolated from indicated

tissues in **e**, control PBS-treated or **f**, DT-treated *Foxp3<sup>DTR</sup>* mice 10 days after Treg cell transfer. **g**, PCA of gene expression by different Treg and Tconv cell subsets. Different cell samples were grouped by treatment (top) or anatomical location (bottom).



**Extended Data Fig. 2 | Tissue Treg cells consistently produced high levels of IL-10 regardless of the presence or absence of inflammatory conditions.**

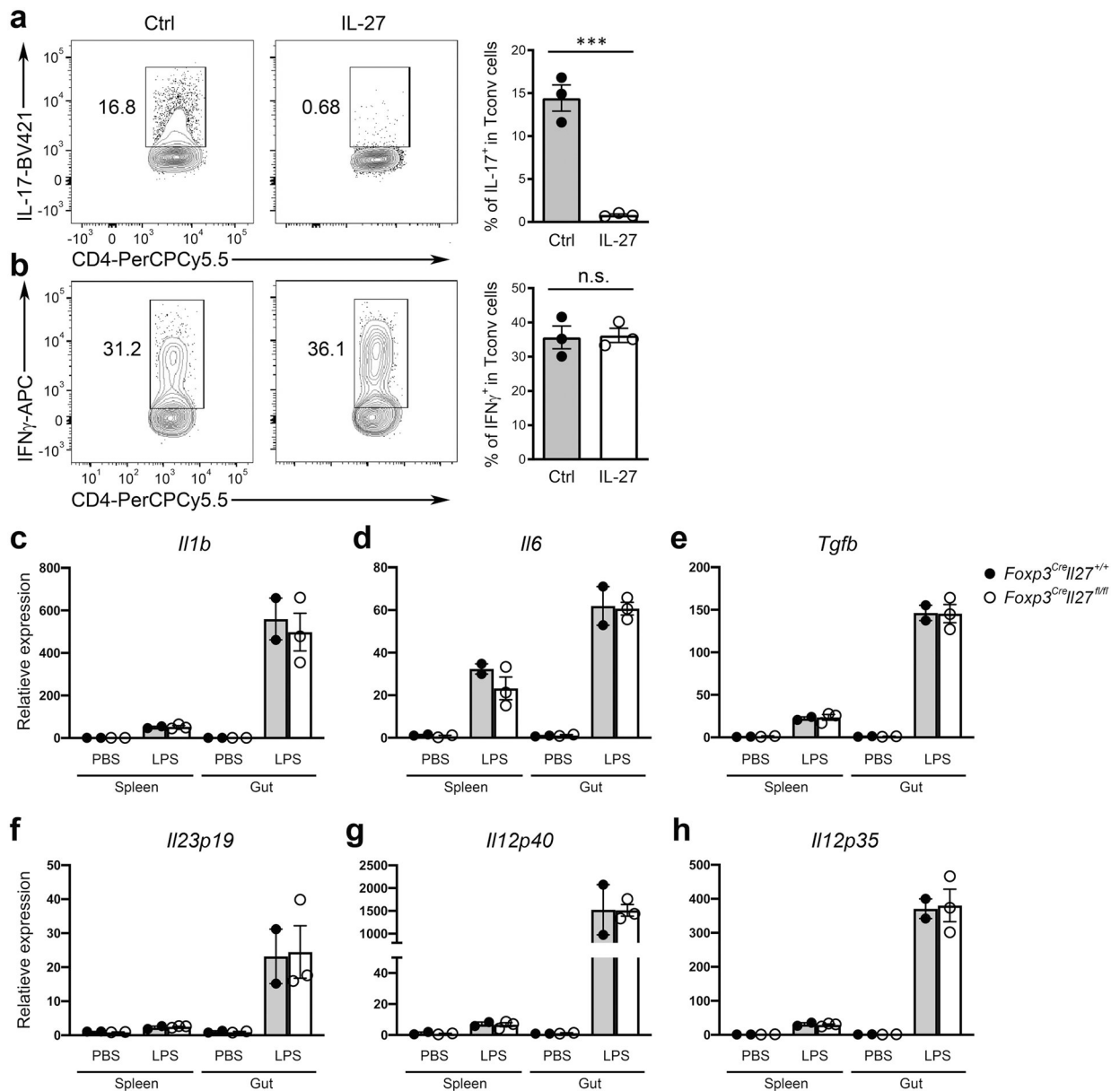
**a**, qPCR analyses for the expressions of *Il10* in Tconv and Treg cells in different tissues from control PBS- or DT-treated *Foxp3<sup>DTR</sup>* mice. Each symbol represents an individual mouse ( $n = 5$ ). **b**, ELISA analyses of the production of IL-10 by Tconv and Treg cells in different tissues from control PBS- or DT-treated *Foxp3<sup>DTR</sup>* mice. Each symbol represents FACS-isolated cell sample pooled from two to three mice ( $n = 4$ ). Dotted line represents the minimum detection limit of the cytokine. Data are presented as mean values  $\pm$  SD. In **a**,  $**P = 0.0021$  (up);  $**P = 0.0084$  (middle); n.s. = 0.4266 (bottom). In **b**,  $**P = 0.0081$  (up),  $*P = 0.0385$  (middle); n.s. = 0.3009 (bottom). Statistical significance was determined by two-tailed unpaired t test.



**Extended Data Fig. 3 | Loss of IL-27 produced by Treg cells did not lead to any obvious immune phenotype except for increased Th17 responses in the intestine.**

Frequencies and numbers of Foxp3<sup>+</sup> Treg cells and frequencies of Ki67<sup>+</sup>, CD44<sup>hi</sup>CD62L<sup>lo</sup>, IL-17<sup>+</sup>, and IFNγ<sup>+</sup> Tconv cells gated on the live CD4<sup>+</sup>Foxp3<sup>-</sup> population in **a**, spleen and **b**, LI LP of *Foxp3<sup>Cre</sup>Il27<sup>fl/fl</sup>* mice and WT littermates (~8–12 weeks). **c**, FACS analysis and **d**, frequencies of RORγt<sup>+</sup> in Tconv cells gated on the live CD4<sup>+</sup>Foxp3<sup>-</sup> population in spleen and SI LP of *Foxp3<sup>Cre</sup>Il27<sup>fl/fl</sup>* mice and WT littermates (~8–12 weeks). **e**, Frequencies of IL-17<sup>+</sup> in RORγt<sup>+</sup> Tconv cells gated on the live CD4<sup>+</sup>Foxp3<sup>-</sup> population in spleen and SI LP of *Foxp3<sup>Cre</sup>Il27<sup>fl/fl</sup>* mice and WT littermates (~8–12 weeks). **f**, Frequencies of IL-17<sup>+</sup> and IFNγ<sup>+</sup> Ly5.1<sup>+</sup> Teff cells (isolated from *Foxp3<sup>KO</sup>* mice) gated on the live CD4<sup>+</sup>Foxp3<sup>-</sup> population in spleens of RAG-deficient mice three weeks after co-transferred with Treg cells isolated from either *Foxp3<sup>Cre</sup>Il27<sup>fl/fl</sup>* mice or WT littermates. Each symbol represents an individual mouse. Data are presented as mean values ± SD. In **a**, from right to left: n.s. = 0.2762 ( $n = 10$  for *Foxp3<sup>Cre</sup>Il27<sup>+/+</sup>*; 8 for *Foxp3<sup>Cre</sup>Il27<sup>fl/fl</sup>*); n.s. = 0.2290 ( $n = 9$  for *Foxp3<sup>Cre</sup>Il27<sup>+/+</sup>*; 7 for *Foxp3<sup>Cre</sup>Il27<sup>fl/fl</sup>*); n.s. = 0.9168 ( $n = 8$  for *Foxp3<sup>Cre</sup>Il27<sup>+/+</sup>*; 7 for *Foxp3<sup>Cre</sup>Il27<sup>fl/fl</sup>*); n.s. = 0.9197 ( $n = 8$  for *Foxp3<sup>Cre</sup>Il27<sup>+/+</sup>*; 7 for *Foxp3<sup>Cre</sup>Il27<sup>fl/fl</sup>*); n.s. = 0.2547 ( $n = 9$  for *Foxp3<sup>Cre</sup>Il27<sup>+/+</sup>*; 7 for *Foxp3<sup>Cre</sup>Il27<sup>fl/fl</sup>*); n.s. = 0.3885 ( $n = 10$  for *Foxp3<sup>Cre</sup>Il27<sup>+/+</sup>*; 8 for *Foxp3<sup>Cre</sup>Il27<sup>fl/fl</sup>*). In **b**, from right to left: n.s. = 0.7752; n.s. = 0.5144; n.s. = 0.5537; n.s. = 0.8933; \* $P = 0.0155$ ; n.s. = 0.0577 ( $n = 8$ ). In **d**, Spl: n.s. = 0.9907; SI: \*\* $P = 0.0025$  ( $n = 7$ ). In **e**, Spl: n.s. = 0.7866; SI: n.s. = 0.4099 ( $n = 7$ ). In **f**,

IL-17: n.s. = 0.7980; IFN $\gamma$ : n.s. = 0.7652 ( $n = 12$ ). Statistical significance was determined by two-tailed unpaired t test.

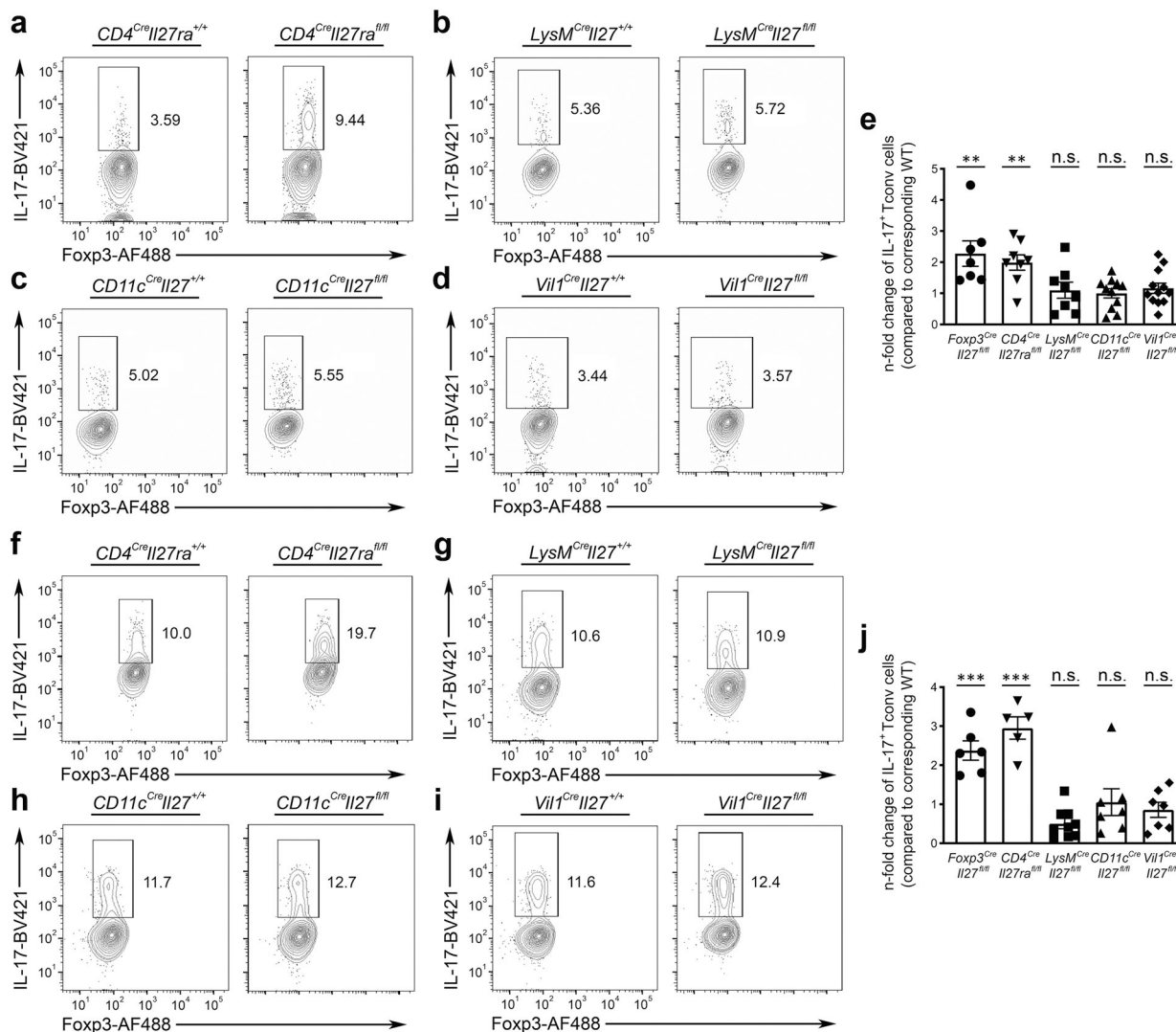


**Extended Data Fig. 4 | Treg cell-derived IL-27 likely limits Th17 responses through directly acting on T cells.**

FACS analysis and frequencies of **a**, IL-17<sup>+</sup> and **b**, IFN $\gamma$ <sup>+</sup> cells in Tconv cells gated on the live CD4<sup>+</sup>Foxp3<sup>-</sup> population cultured in the presence or absence of IL-27 (100 ng/ml) under Th17 and Th1 polarizing conditions, respectively. Each symbol represents an individual experiment ( $n = 3$ ). qPCR analyses for the expressions of **c**, *Il1b*, **d**, *Il6*, **e**, *Tgfb*, **f**, *Il23p19*, **g**, *Il12p40*, and **h**, *Il12p35* in DCs isolated from SI LP of either *Foxp3*<sup>Cre</sup>*Il27*<sup>fl/fl</sup> mice or WT littermates. Each symbol represents FACS-isolated cell sample pooled from two to three



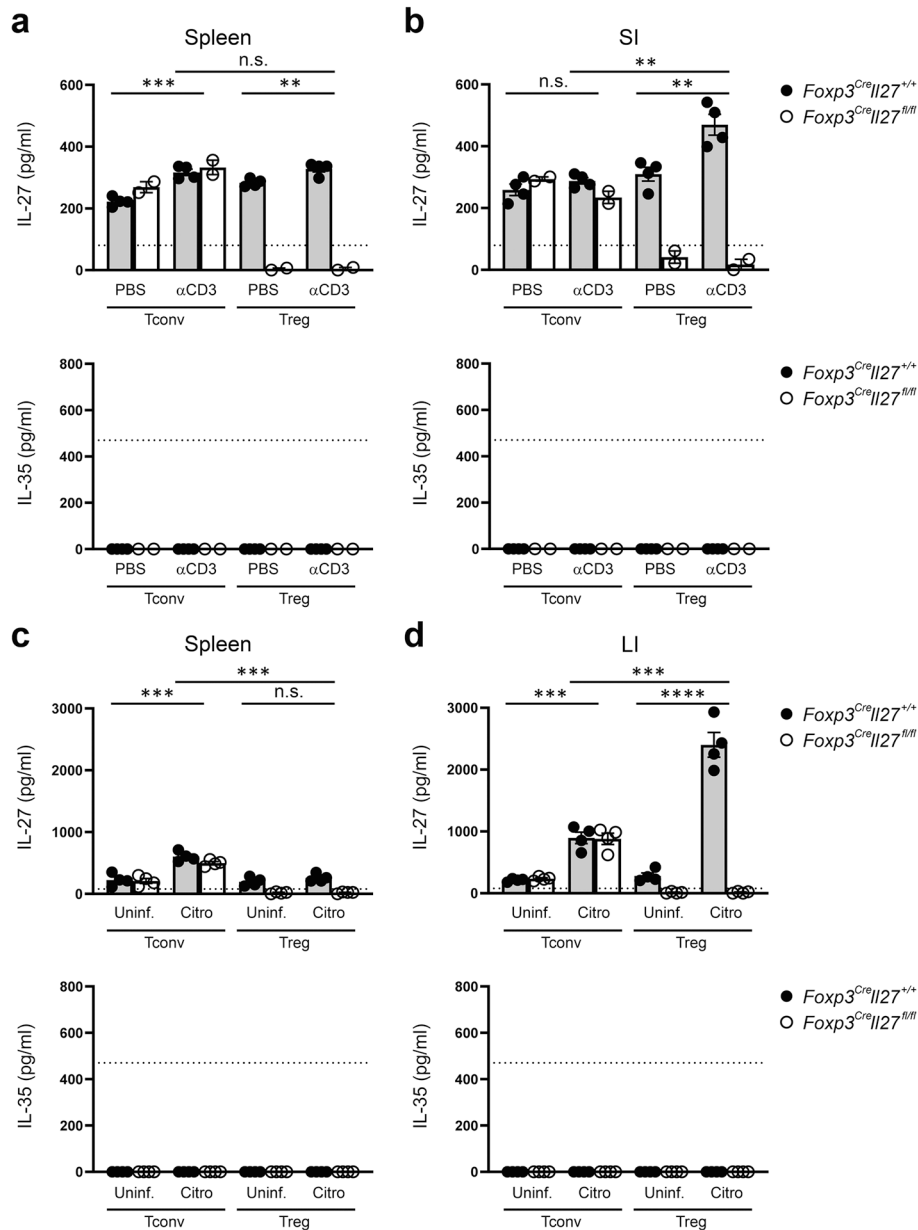
mice ( $n = 2$ ). Data are presented as mean values  $\pm$  SD. In **a**,  $***P = 0.0009$ . In **b**,  $n.s. = 0.8920$ . Statistical significance was determined by two-tailed unpaired t test.



**Extended Data Fig. 5 | IL-27 produced by other non-Treg intestinal resident cell types is not required for IL-27-mediated regulation of Th17 responses.**

FACS analysis of IL-17<sup>+</sup> Tconv cells gated on the live CD4<sup>+</sup>Foxp3<sup>-</sup> population in SI LP of **a**, *CD4<sup>Cre</sup>Il27ra<sup>fl/fl</sup>* mice, **b**, *LysM<sup>Cre</sup>Il27<sup>fl/fl</sup>*, **c**, *CD11c<sup>Cre</sup>Il27<sup>fl/fl</sup>*, **d**, *Vil1<sup>Cre</sup>Il27<sup>fl/fl</sup>*, and their corresponding WT littermates ( $\sim 8$ – $12$  weeks). **e**, n-fold changes (on the basis of corresponding WT controls) of IL-17<sup>+</sup> Tconv cell frequencies in indicated mouse lines. FACS analysis of IL-17<sup>+</sup> Tconv cells gated on the live CD4<sup>+</sup>Foxp3<sup>-</sup> population in SI LP of **f**, *CD4<sup>Cre</sup>Il27ra<sup>fl/fl</sup>* mice **g**, *LysM<sup>Cre</sup>Il27<sup>fl/fl</sup>*, **h**, *CD11c<sup>Cre</sup>Il27<sup>fl/fl</sup>*, **i**, *Vil1<sup>Cre</sup>Il27<sup>fl/fl</sup>*, and their corresponding WT littermates 4 days after initial aCD3 mAb injection. **j**, n-fold changes (on the basis of corresponding WT controls) of IL-17<sup>+</sup> Tconv cell frequencies in indicated mouse lines. Each symbol represents an individual mouse. Data are presented as mean values  $\pm$  SD. In **e**, from left to right:  $***P = 0.0065$  ( $n = 7$ );  $***P = 0.006$  ( $n = 8$ );  $n.s. = 0.7795$  ( $n = 8$ );  $n.s. = 0.7158$  ( $n = 11$ );  $n.s. = 0.5244$  ( $n = 12$ ). In **j**, from left to right:  $***P$

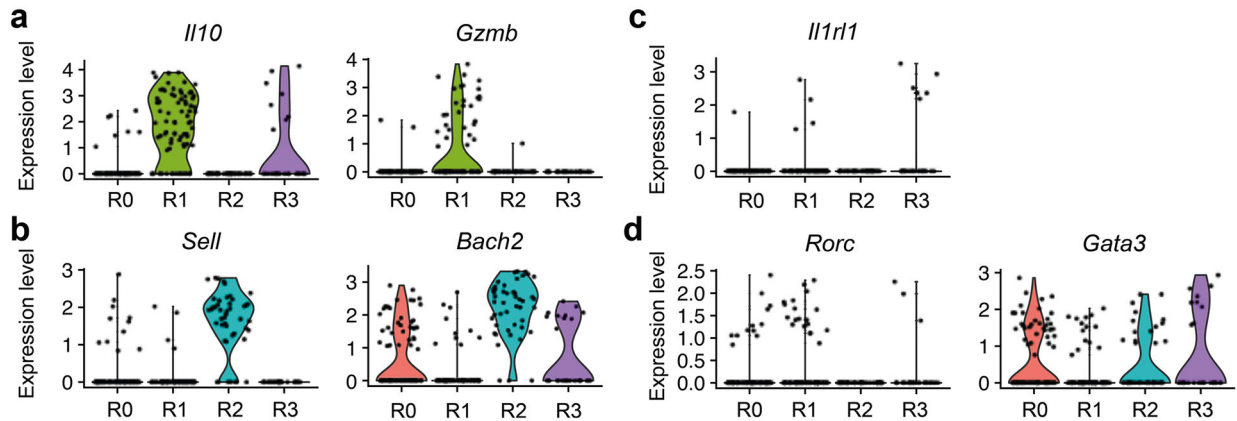
= 0.001 ( $n = 6$ ); \*\*\* $P = 0.001$  ( $n = 5$ ); n.s. = 0.1755 ( $n = 9$ ); n.s. = 0.6306 ( $n = 7$ ); n.s. = 0.4163 ( $n = 7$ ). Statistical significance was determined by two-tailed unpaired t test.



**Extended Data Fig. 6 |. Elevated IL-27 production by intestinal Treg cells could be observed in other autoimmune- and infection-driven inflammatory settings.**

ELISA analyses of the production of IL-27 or IL-35 by Tconv and Treg cells in **a**, spleen and **b**, SI LP from PBS or  $\alpha$ CD3 mAb treated *Foxp3<sup>Cre</sup>Il27<sup>fl/fl</sup>* mice and WT littermates. Each symbol represents FACS-isolated cell sample pooled from two to three mice ( $n = 4$  for *Foxp3<sup>Cre</sup>Il27<sup>+/+</sup>*; 2 for *Foxp3<sup>Cre</sup>Il27<sup>fl/fl</sup>*). ELISA analyses of the production of IL-27 or IL-35 by Tconv and Treg cells in **c**, spleen and **d**, LI LP from *Foxp3<sup>Cre</sup>Il27<sup>fl/fl</sup>* mice and WT littermates at day 10 post *C. rodentium* infection. Each symbol represents FACS-isolated cell sample pooled from two to three mice ( $n = 4$ ). Dotted line represents the minimum detection

limit of the indicated cytokine. Data are presented as mean values  $\pm$  SD. In **a**, n.s. = 0.4560 (top); \*\*\* $P$  = 0.0003 (bottom left); \*\* $P$  = 0.0090 (bottom right). In **b**, \*\* $P$  = 0.0021 (top); n.s. = 0.2264 (bottom left); \*\* $P$  = 0.0074 (bottom right). In **c**, \*\*\* $P$  = 0.0005 (top), \*\*\* $P$  = 0.0010 (bottom left), n.s. = 0.2535 (bottom right). In **d**, \*\*\* $P$  = 0.0005 (top), \*\*\* $P$  = 0.0003 (bottom left), \*\*\*\* $P$  < 0.0001 (bottom right). Statistical significance was determined by two-tailed unpaired t test.



**Extended Data Fig. 7 | Expression of known intestinal Treg cell markers in different Treg cell clusters.**

Violin plots of **a**, *Il10* and *Gzmb*, **b**, *Sell* and *Bach2*, **c**, *Il1r1*, and **d**, *Rorc* and *Gata3* in different intestinal Treg cell clusters from *C. rodentium*-infected mice.

## Acknowledgements

The present study was supported by the NIH (grant nos. AI108651, AI127751 and AI163813 to L.-F.L., DK110534 and DK120515 to H.C., AI126277, AI145325 and AI154644 to M.R. and AI132122 and BX005106 to J.T.C.). Work in M.R.'s laboratory is also supported by the University of California, San Diego, Center for Mucosal Immunology, Allergy, and Vaccines, Chiba University. M.R. holds an Investigator in the Pathogenesis of Infectious Disease Award from the Burroughs Wellcome Fund. R.P. is a BioLegend fellow. R.R.G. is partly supported by a fellowship from the Crohn's and Colitis Foundation. We thank all members of our laboratory for discussions.

## Competing interests

L.-F.L. is a scientific advisor for Elixiron Immunotherapeutics and receives research grants from AstraZeneca, Avidity Biosciences and Molecular Axiom. E.I., J.B., M.N., M.C. and R.A.M are or were employees of AstraZeneca and may own stock or stock options. As such, they declare that they are bound by confidentiality agreements that prevent them from disclosing their competing interests in this work. The remaining authors declare no competing interests.

## Data availability

All data are present in the article and supplementary information files are available from the corresponding authors upon reasonable request. RNA-seq data underlying Figs. 1 and 2 and Extended Data Fig. 1, as well as scRNA-seq data underlying Fig. 7 and Extended Data Fig. 7, are available from the National Center for Biotechnology Information under accession no. [GSE217949](https://www.ncbi.nlm.nih.gov/geo/query/acc.cgi?acc=GSE217949). Source data are provided with this paper.

## References

1. Josefowicz SZ, Lu LF & Rudensky AY Regulatory T cells: mechanisms of differentiation and function. *Annu. Rev. Immunol* 30, 531–564 (2012). [PubMed: 22224781]
2. Campbell DJ & Koch MA Phenotypical and functional specialization of FOXP3+ regulatory T cells. *Nat. Rev. Immunol* 11, 119–130 (2011). [PubMed: 21267013]
3. Munoz-Rojas AR & Mathis D Tissue regulatory T cells: regulatory chameleons. *Nat. Rev. Immunol* 21, 597–611 (2021). [PubMed: 33772242]
4. Arpaia N et al. A distinct function of regulatory T cells in tissue protection. *Cell* 162, 1078–1089 (2015). [PubMed: 26317471]
5. Burzyn D et al. A special population of regulatory T cells potentiates muscle repair. *Cell* 155, 1282–1295 (2013). [PubMed: 24315098]
6. Ito M et al. Brain regulatory T cells suppress astrogliosis and potentiate neurological recovery. *Nature* 565, 246–250 (2019). [PubMed: 30602786]
7. Li Y et al. Insulin signaling establishes a developmental trajectory of adipose regulatory T cells. *Nat. Immunol* 22, 1175–1185 (2021). [PubMed: 34429546]
8. Rubtsov YP et al. IL-10 produced by regulatory T cells contributes to their suppressor function by limiting inflammation at environmental interfaces. *Immunity* 28, 546–558 (2008). [PubMed: 18387831]
9. Wei X et al. Reciprocal expression of IL-35 and IL-10 defines two distinct effector treg subsets that are required for maintenance of immune tolerance. *Cell Rep.* 21, 1853–1869 (2017). [PubMed: 29141218]
10. Yoshida H & Hunter CA The immunobiology of interleukin-27. *Annu. Rev. Immunol* 33, 417–443 (2015). [PubMed: 25861977]
11. Cretney E, Kallies A & Nutt SL Differentiation and function of Foxp3<sup>+</sup> effector regulatory T cells. *Trends Immunol.* 34, 74–80 (2013). [PubMed: 23219401]
12. Levine AG, Arvey A, Jin W & Rudensky AY Continuous requirement for the TCR in regulatory T cell function. *Nat. Immunol* 15, 1070–1078 (2014). [PubMed: 25263123]
13. Kim JM, Rasmussen JP & Rudensky AY Regulatory T cells prevent catastrophic autoimmunity throughout the lifespan of mice. *Nat. Immunol* 8, 191–197 (2007). [PubMed: 17136045]
14. Batten M et al. Interleukin 27 limits autoimmune encephalomyelitis by suppressing the development of interleukin 17-producing T cells. *Nat. Immunol* 7, 929–936 (2006). [PubMed: 16906167]
15. Stumhofer JS et al. Interleukin 27 negatively regulates the development of interleukin 17-producing T helper cells during chronic inflammation of the central nervous system. *Nat. Immunol* 7, 937–945 (2006). [PubMed: 16906166]
16. Awasthi A et al. A dominant function for interleukin 27 in generating interleukin 10-producing anti-inflammatory T cells. *Nat. Immunol* 8, 1380–1389 (2007). [PubMed: 17994022]
17. Hall AO et al. The cytokines interleukin 27 and interferon-gamma promote distinct Treg cell populations required to limit infection-induced pathology. *Immunity* 37, 511–523 (2012). [PubMed: 22981537]
18. Collison LW et al. The inhibitory cytokine IL-35 contributes to regulatory T-cell function. *Nature* 450, 566–569 (2007). [PubMed: 18033300]
19. Merger M et al. Defining the roles of perforin, Fas/FasL, and tumour necrosis factor alpha in T cell induced mucosal damage in the mouse intestine. *Gut* 51, 155–163 (2002). [PubMed: 12117872]
20. Lin CH et al. Gut epithelial IL-27 confers intestinal immunity through the induction of intraepithelial lymphocytes. *J. Exp. Med* 218, e20210021 (2021). [PubMed: 34554189]
21. Esplugues E et al. Control of TH17 cells occurs in the small intestine. *Nature* 475, 514–518 (2011). [PubMed: 21765430]
22. Xu ZS et al. FAM64A positively regulates STAT3 activity to promote Th17 differentiation and colitis-associated carcinogenesis. *Proc. Natl Acad. Sci. USA* 116, 10447–10452 (2019). [PubMed: 31061131]

23. Pastille E et al. Transient ablation of regulatory T cells improves antitumor immunity in colitis-associated colon cancer. *Cancer Res.* 74, 4258–4269 (2014). [PubMed: 24906621]
24. Korn T & Kallies A T cell responses in the central nervous system. *Nat. Rev. Immunol* 17, 179–194 (2017). [PubMed: 28138136]
25. Khader SA, Gaffen SL & Kolls JK Th17 cells at the crossroads of innate and adaptive immunity against infectious diseases at the mucosa. *Mucosal Immunol.* 2, 403–411 (2009). [PubMed: 19587639]
26. Ishigame H et al. Differential roles of interleukin-17A and –17F in host defense against mucoc epithelial bacterial infection and allergic responses. *Immunity* 30, 108–119 (2009). [PubMed: 19144317]
27. Kimura D et al. Interleukin-27-producing CD4<sup>+</sup> T cells regulate protective immunity during malaria parasite infection. *Immunity* 44, 672–682 (2016). [PubMed: 26968425]
28. Dupont CD, Christian DA & Hunter CA Immune response and immunopathology during toxoplasmosis. *Semin. Immunopathol* 34, 793–813 (2012). [PubMed: 22955326]
29. Tanoue T, Atarashi K & Honda K Development and maintenance of intestinal regulatory T cells. *Nat. Rev. Immunol* 16, 295–309 (2016). [PubMed: 27087661]
30. Yang BH et al. TCF1 and LEF1 control Treg competitive survival and Tfr development to prevent autoimmune diseases. *Cell Rep.* 27, 3629–3645.e3626 (2019). [PubMed: 31216480]
31. Miragaia RJ et al. Single-cell transcriptomics of regulatory T cells reveals trajectories of tissue adaptation. *Immunity* 50, 493–504.e497 (2019). [PubMed: 30737144]
32. Grant FM et al. BACH2 drives quiescence and maintenance of resting Treg cells to promote homeostasis and cancer immunosuppression. *J. Exp. Med* 217, e20190711 (2020). [PubMed: 32515782]
33. Rao DA, Arazi A, Wofsy D & Diamond B Design and application of single-cell RNA sequencing to study kidney immune cells in lupus nephritis. *Nat. Rev. Nephrol* 16, 238–250 (2020). [PubMed: 31853010]
34. Kreiser S et al. Murine CD83-positive T cells mediate suppressor functions in vitro and in vivo. *Immunobiology* 220, 270–279 (2015). [PubMed: 25151500]
35. Liu J, Guan X & Ma X Regulation of IL-27 p28 gene expression in macrophages through MyD88- and interferon-gamma-mediated pathways. *J. Exp. Med* 204, 141–152 (2007). [PubMed: 17227910]
36. Wang S et al. MyD88 adaptor-dependent microbial sensing by regulatory T cells promotes mucosal tolerance and enforces commensalism. *Immunity* 43, 289–303 (2015). [PubMed: 26231118]
37. Villarino A et al. The IL-27R (WSX-1) is required to suppress T cell hyperactivity during infection. *Immunity* 19, 645–655 (2003). [PubMed: 14614852]
38. Takeda A et al. Cutting edge: role of IL-27/WSX-1 signaling for induction of T-bet through activation of STAT1 during initial Th1 commitment. *J. Immunol* 170, 4886–4890 (2003). [PubMed: 12734330]
39. Lee HM et al. IFN $\gamma$  signaling endows DCs with the capacity to control type I inflammation during parasitic infection through promoting T-bet<sup>+</sup> regulatory T cells. *PLoS Pathog.* 11, e1004635 (2015). [PubMed: 25658840]
40. Ohnmacht C et al. MUCOSAL IMMUNOLOGY. The microbiota regulates type 2 immunity through ROR $\gamma$ mat<sup>+</sup> T cells. *Science* 349, 989–993 (2015). [PubMed: 26160380]
41. Sefik E et al. MUCOSAL IMMUNOLOGY. Individual intestinal symbionts induce a distinct population of ROR $\gamma$ mat<sup>+</sup> regulatory T cells. *Science* 349, 993–997 (2015). [PubMed: 26272906]
42. Andrews C, McLean MH & Durum SK Interleukin-27 as a novel therapy for inflammatory bowel disease: a critical review of the literature. *Inflamm. Bowel Dis* 22, 2255–2264 (2016). [PubMed: 27243591]
43. Imielinski M et al. Common variants at five new loci associated with early-onset inflammatory bowel disease. *Nat. Genet* 41, 1335–1340 (2009). [PubMed: 19915574]
44. Cox JH et al. IL-27 promotes T cell-dependent colitis through multiple mechanisms. *J. Exp. Med* 208, 115–123 (2011). [PubMed: 21173106]

45. Visperas A, Do JS, Bulek K, Li X & Min B IL-27, targeting antigen-presenting cells, promotes Th17 differentiation and colitis in mice. *Mucosal Immunol.* 7, 625–633 (2014). [PubMed: 24129161]
46. Fontenot JD, Gavin MA & Rudensky AY Foxp3 programs the development and function of CD4+ CD25+ regulatory T cells. *Nat. Immunol* 4, 330–336 (2003). [PubMed: 12612578]
47. Liston A et al. Differentiation of regulatory Foxp3+ T cells in the thymic cortex. *Proc. Natl Acad. Sci. USA* 105, 11903–11908 (2008). [PubMed: 18695219]
48. Crepin VF, Collins JW, Habibzay M & Frankel G *Citrobacter rodentium* mouse model of bacterial infection. *Nat. Protoc* 11, 1851–1876 (2016). [PubMed: 27606775]
49. Thaker AI, Shaker A, Rao MS & Ciorba MA Modeling colitis-associated cancer with azoxymethane (AOM) and dextran sulfate sodium (DSS). *J. Vis. Exp* 67, 4100 (2012).
50. Hu S et al. cGAS restricts colon cancer development by protecting intestinal barrier integrity. *Proc. Natl Acad. Sci. USA* 118, e2105747118 (2021). [PubMed: 34074794]



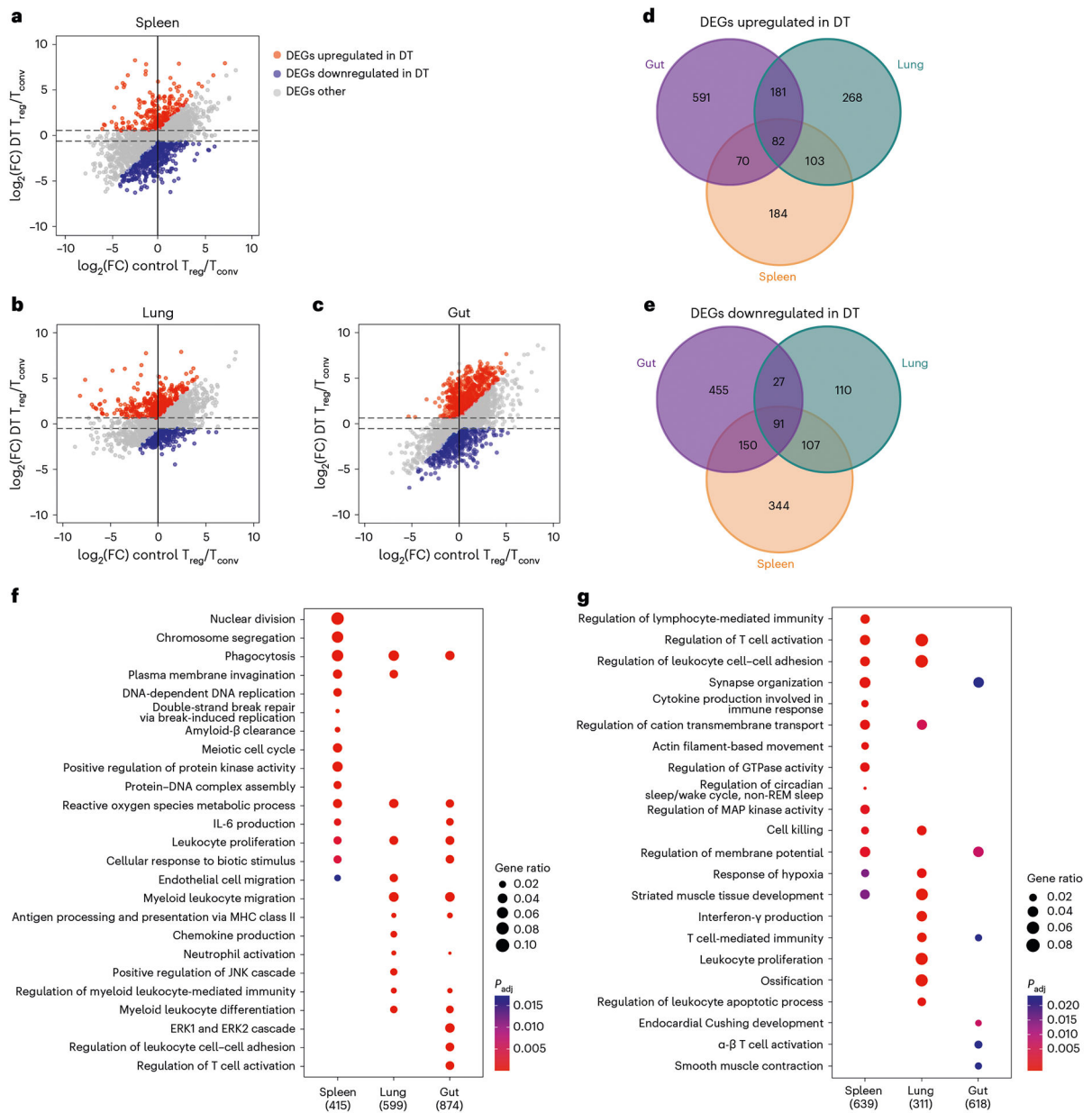


**Fig. 1 |. Transcriptomic analysis of tissue  $T_{reg}$  cells during active suppression of local inflammatory responses.**

**a–c**, Scatter plots depicting  $\log_2(\text{fold-change})$  ( $\log_2(\text{FC})$ ) of gene expression in spleen (**a**), lung (**b**) and gut (SI LP) (**c**) of  $T_{reg}$  cells over  $T_{conv}$  cells in DT-treated mice versus those in PBS-treated controls. Genes that are upregulated under DT-treated condition (false discovery rate (FDR) < 5% and the value of  $\log_2(\text{FC}) > 0.585$  (1.5-fold) and at least 0.585 higher than the value of  $\log_2(\text{FC})$  under the PBS-treated control condition). Genes are downregulated under the DT-treated condition (FDR < 5% and the value of  $\log_2(\text{FC}) < -0.585$  and at least 0.585 lower than the value of  $\log_2(\text{FC})$  under the PBS-treated control condition).

**d,g**, Venn diagrams demonstrating genes upregulated (**d**) or downregulated (**e**) in different tissue-specific  $T_{reg}$  cells from DT-treated mice. Numbers represent gene numbers. **f,g**, Dot plot of GO term enrichment analysis of DEGs upregulated (**f**) or downregulated (**g**) in tissue

T<sub>reg</sub> cell subsets. MHC, Major histocompatibility complex; REM, rapid eye movement. Colors indicate the *P* values from Fisher's exact test and dot size is proportional to the number of DEGs in a given biological process.

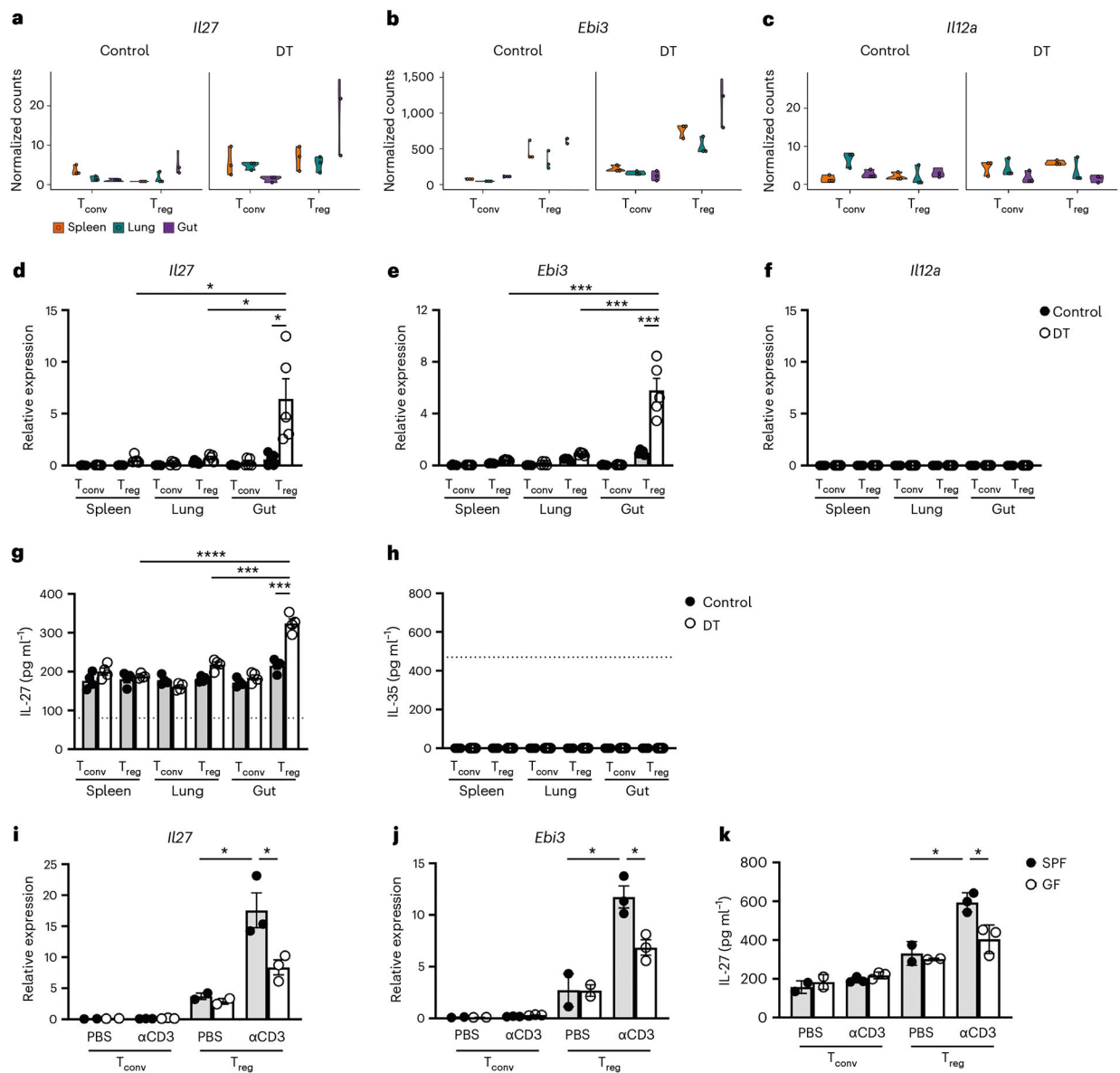


**Fig. 2 | Identification of IL-27 not IL-35 as a potential suppressor molecule specifically produced by intestinal T<sub>reg</sub> cells under autoimmune inflammation.**

**a–c**, Violin plots of *Il27* (**a**), *Ebi3* (**b**) and *Il12a* (**c**) in T<sub>conv</sub> and T<sub>reg</sub> cells in different tissues from control PBS- or DT-treated *Foxp3<sup>DTR</sup>* mice by RNA-seq analysis. **d–f**, The qPCR analyses for the expression of *Il27* (**d**), *Ebi3* (**e**) and *Il12a* (**f**) in T<sub>conv</sub> and T<sub>reg</sub> cells in different tissues from control PBS- or DT-treated mice. Each symbol represents an individual mouse ( $n = 5$ ). **g,h**, ELISA of the production of IL-27 (**g**) or IL-35 (**h**) by T<sub>conv</sub> and T<sub>reg</sub> cells in different tissues from control PBS- or DT-treated mice. **i,j**, The qPCR analyses for the expressions of *Il27* (**i**) and *Ebi3* (**j**) in T<sub>conv</sub> and T<sub>reg</sub> cells in SI from control PBS- or aCD3<sup>-</sup>-treated SPF or GF mice. Each symbol represents a FACS-isolated cell sample pooled from two to three mice ( $n = 4$ ). **k**, ELISA analyses of the production of IL-27 by T<sub>conv</sub> and T<sub>reg</sub> cells in SI LP from control PBS- or aCD3 monoclonal antibody-treated SPF and GF mice. Each symbol represents a FACS-isolated cell sample pooled from two

to three mice ( $n = 2$  for SPF and 3 for GF). The dotted line represents the minimum detection limit of the indicated cytokine. The data are presented as mean values  $\pm$  s.d. In **d**,  $*P = 0.0164$  (up), 0.0187 (middle) and 0.0173 (bottom). In **e**,  $***P = 0.0004$  (up), 0.0007 (middle) and 0.0008 (bottom). In **g**,  $****P < 0.0001$  (top), 0.0003 (middle) and 0.0003 (bottom). In **i**,  $*P = 0.0351$  (left) and 0.0394 (right). In **j**,  $*P = 0.0467$  (left) and 0.0193 (right). In **k**,  $*P = 0.0413$  (left) and 0.0207 (right). Statistical significance was determined using a two-tailed, unpaired Student's *t*-test.

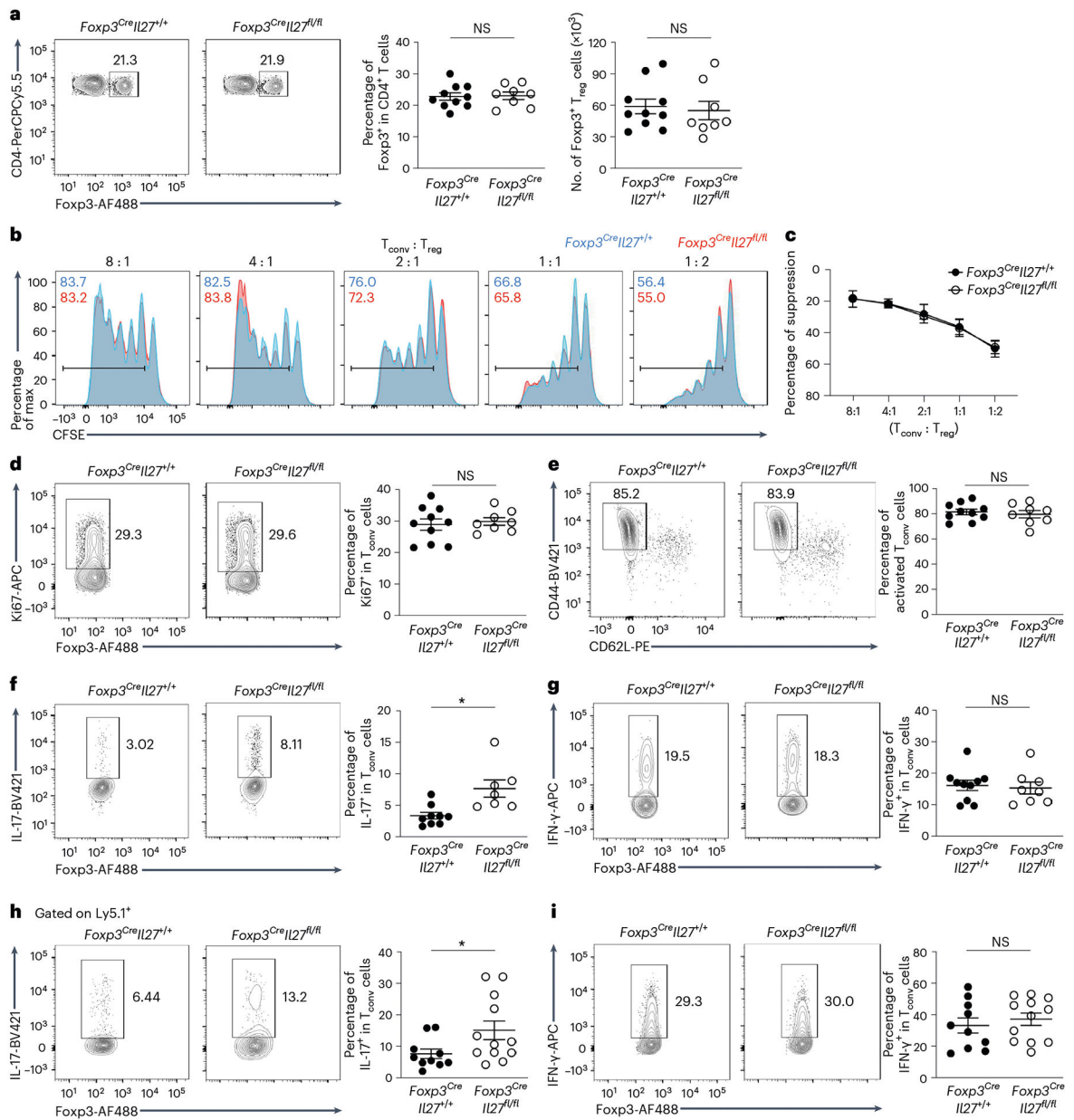


**Fig. 3 | A selective defect in regulating intestinal T<sub>H</sub>17 cell responses in mice harboring T<sub>reg</sub> cells incapable of producing IL-27.**

**a**, FACS analysis, frequencies and numbers of Foxp3<sup>+</sup> T<sub>reg</sub> cells gated on the live CD4<sup>+</sup> population in SI LP of *Foxp3<sup>Cre</sup> Il27<sup>fl/fl</sup>* mice and WT littermates (age ~8–12 weeks). Each symbol represents an individual mouse ( $n = 10$  for *Foxp3<sup>Cre</sup> Il27<sup>+/+</sup>* and 8 for *Foxp3<sup>Cre</sup> Il27<sup>fl/fl</sup>*). **b,c**, FACS analysis (**b**) and percentage of suppression of proliferation (**c**) of WT T<sub>conv</sub> cells by SI LP T<sub>reg</sub> cells isolated from either WT or *Foxp3<sup>Cre</sup> Il27<sup>fl/fl</sup>* mice in an in vitro suppression assay. Data represent three independent experiments ( $n = 2$ ). **d–g**, FACS analysis and frequencies of Ki67<sup>+</sup> (**d**), CD44<sup>hi</sup>CD62L<sup>lo</sup> (**e**), IL-17<sup>+</sup> (**f**) and IFN-γ<sup>+</sup> T<sub>conv</sub> (**g**) cells gated on the live CD4<sup>+</sup>Foxp3<sup>+</sup> population in SI LP of *Foxp3<sup>Cre</sup> Il27<sup>fl/fl</sup>* mice and WT littermates (age ~8–12 weeks). Each symbol represents an individual mouse ( $n = 10$  for *Foxp3<sup>Cre</sup> Il27<sup>+/+</sup>* and 8 for *Foxp3<sup>Cre</sup> Il27<sup>fl/fl</sup>*). **h,i**, FACS analysis and frequencies of

IL-17<sup>+</sup> (**h**) and IFN- $\gamma$ <sup>+</sup>Ly5.1<sup>+</sup> (**i**) T<sub>eff</sub> cells (isolated from Ly5.1<sup>+</sup>*Foxp3*<sup>KO</sup> mice) gated on the live CD4<sup>+</sup> population in SI LP of RAG-deficient mice 3 weeks after being co-transferred with T<sub>reg</sub> cells isolated from either *Foxp3*<sup>Cre</sup>*Il27*<sup>fl/fl</sup> mice or WT littermates. Each symbol represents an individual mouse ( $n = 10$  for *Foxp3*<sup>Cre</sup>*Il27*<sup>+/+</sup> and 12 for *Foxp3*<sup>Cre</sup>*Il27*<sup>fl/fl</sup>). Data are presented as mean values  $\pm$  s.d. In **a**, NS (not significant) = 0.8805 (left) and 0.7346 (right). In **d**, NS = 0.6613. In **e**, NS = 0.6285. In **f**, \* $P = 0.0196$ . In **g**, NS = 0.7544. In **h**, \* $P = 0.0391$ . In **i**, NS = 0.5283. Statistical significance was determined using a two-tailed, unpaired Student's *t*-test.



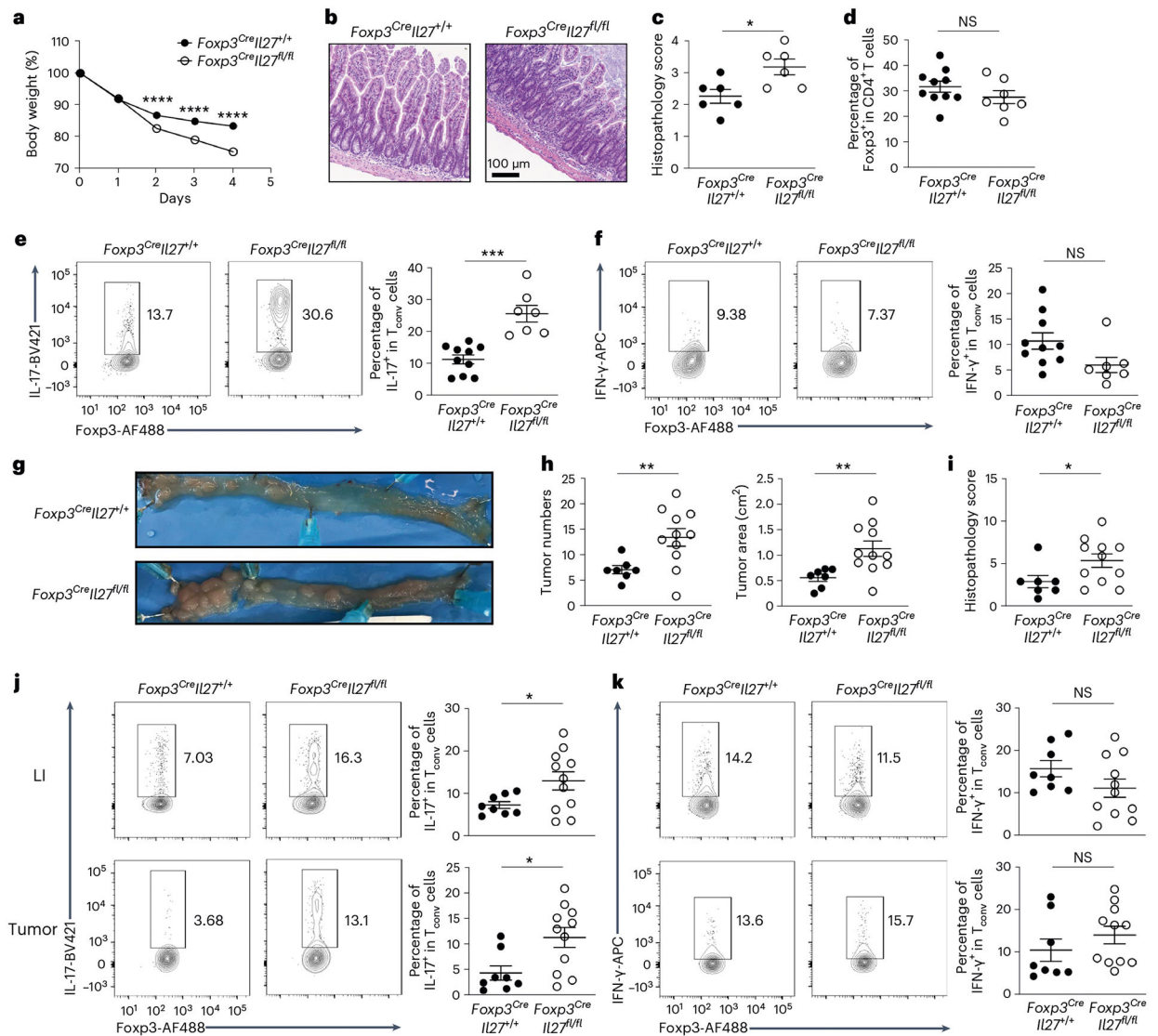


**Fig. 4 | Loss of  $T_{reg}$  cell-derived IL-27 led to exacerbated intestinal inflammation and colitis-associated cancer.**

**a**, Percentage of body weight change of  $Foxp3^{Cre}Il27^{fl/fl}$  mice and WT littermates after aCD3 monoclonal antibody administration. Each symbol represents the average of mice from four independent experiments ( $n = 16$  for  $Foxp3^{Cre}Il27^{+/+}$  and 18 for  $Foxp3^{Cre}Il27^{fl/fl}$ ). **b**, Four days after initial aCD3 monoclonal antibody injection, small intestine sections from the mice were stained with H&E for microscopic imaging. Scale bar, 100  $\mu$ m. Data represent four independent experiments. **c**, Semiquantitative scoring of histopathology. Each symbol represents an individual mouse ( $n = 6$ ). **d-f**, FACS analysis and frequencies of  $Foxp3^+$   $T_{reg}$  cells (**d**),  $IL-17^+$   $T_{conv}$  cells (**e**) and  $IFN-\gamma^+$   $T_{conv}$  cells (**f**) gated on the live  $CD4^+$   $Foxp3^-$  population in SI LP of aCD3 monoclonal antibody-treated  $Foxp3^{Cre}Il27^{fl/fl}$  mice and WT littermates. Each symbol represents an individual mouse ( $n = 10$  for  $Foxp3^{Cre}Il27^{+/+}$  and 7 for  $Foxp3^{Cre}Il27^{fl/fl}$ ). **g**, Representative colonic photos from  $Foxp3^{Cre}Il27^{fl/fl}$  mice and WT littermates 12 weeks after AOM/DSS treatment. Data represent three independent experiments. **h**, Numbers and area of colorectal tumors in

*Foxp3<sup>Cre</sup>Il27<sup>fl/fl</sup>* mice and WT littermates. **i**, Semiquantitative scoring of histopathology. Each symbol represents an individual mouse ( $n = 7$  for *Foxp3<sup>Cre</sup>Il27<sup>+/+</sup>* and 11 for *Foxp3<sup>Cre</sup>Il27<sup>fl/fl</sup>*). **j,k**, FACS analysis and frequencies of IL-17<sup>+</sup> (**j**) and IFN- $\gamma$ <sup>+</sup> (**k**) T<sub>conv</sub> cells gated on the live CD4<sup>+</sup>Foxp3<sup>-</sup> population in LI LP or colorectal tumors of *Foxp3<sup>Cre</sup>Il27<sup>fl/fl</sup>* mice and WT littermates 12 weeks after AOM/DSS treatment. Each symbol represents an individual mouse ( $n = 8$  for *Foxp3<sup>Cre</sup>Il27<sup>+/+</sup>* and 11 for *Foxp3<sup>Cre</sup>Il27<sup>fl/fl</sup>*). Data are presented as mean values  $\pm$  s.d. In **a**, \*\*\*\* $P < 0.0001$ . In **c**, \* $P = 0.0187$ . In **d**, NS = 0.2424. In **e**, \*\*\* $P = 0.0008$ . In **f**, NS = 0.05. In **h**, \*\* $P = 0.0051$  (left) and 0.004 (right). In **i**, \* $P = 0.0363$ . In **j**, \* $P = 0.0278$  (up) and 0.0101 (bottom). In **k**, NS = 0.1307 (up) and 0.3073 (bottom). Statistical significance was determined using a two-tailed, unpaired Student's *t*-test.

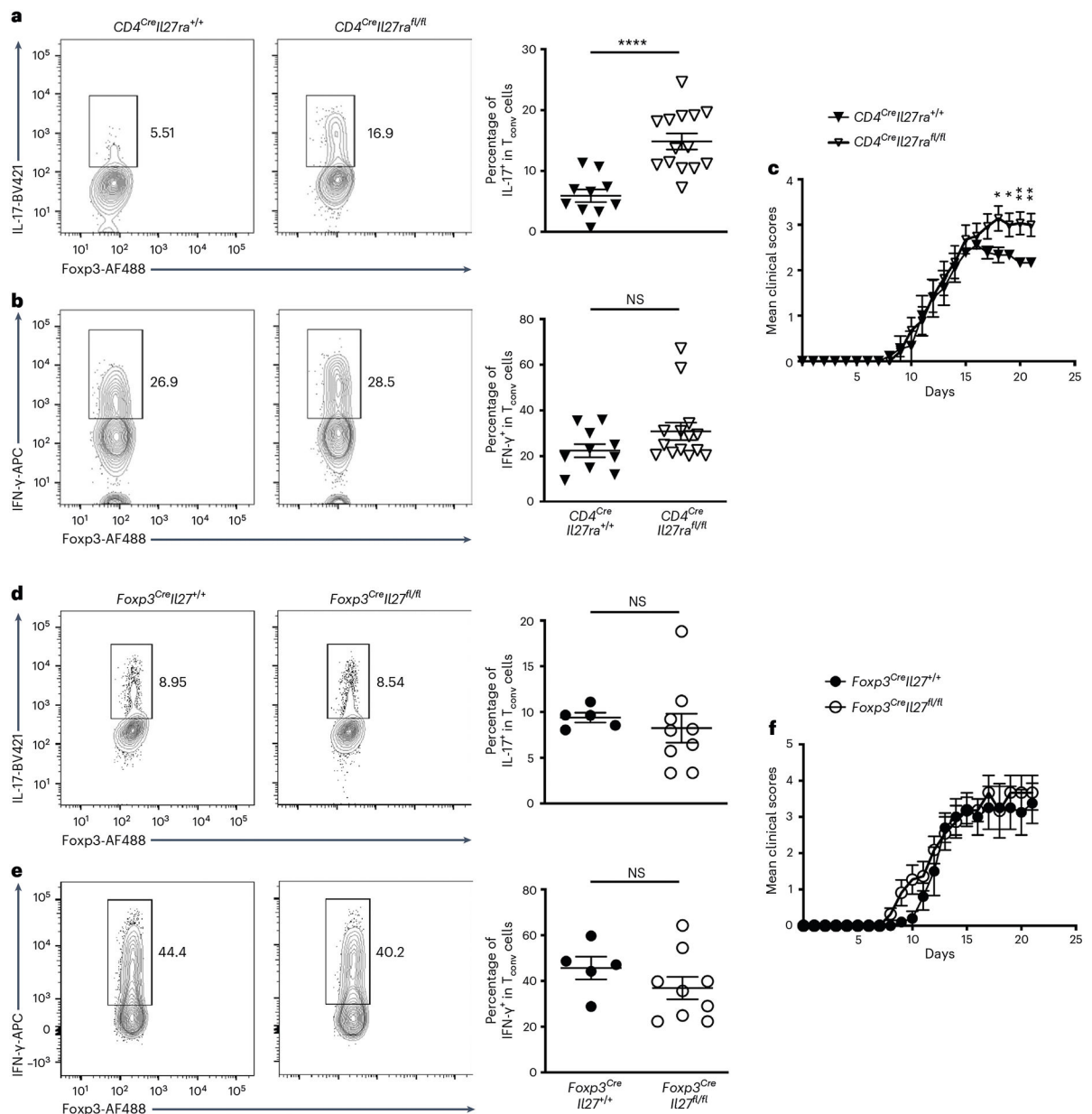


**Fig. 5 | T<sub>reg</sub> cell-derived IL-27 is dispensable for controlling T<sub>H</sub>17 cell-driven EAE.**  
**a,b,** FACS analysis and frequencies of IL-17<sup>+</sup> (**a**) and IFN-γ<sup>+</sup> (**b**) T<sub>conv</sub> cells gated on the live CD4<sup>+</sup>Fopx3<sup>-</sup> population in the brain of *CD4<sup>Cre</sup>IL27ra<sup>fl/fl</sup>* mice and WT littermates 21 d after EAE induction. Each symbol represents an individual mouse ( $n = 10$  for *CD4<sup>Cre</sup>IL27ra<sup>+/+</sup>* and 14 for *CD4<sup>Cre</sup>IL27ra<sup>fl/fl</sup>*). **c,** The disease severity scored regularly based on clinical symptoms. Each symbol represents the average of mice from three independent experiments ( $n = 9$  for *CD4<sup>Cre</sup>IL27ra<sup>+/+</sup>* and 14 for *CD4<sup>Cre</sup>IL27ra<sup>fl/fl</sup>*). **d,e,** FACS analysis and frequencies of IL-17<sup>+</sup> (**d**) and IFN-γ<sup>+</sup> (**e**) T<sub>conv</sub> cells gated on the live CD4<sup>+</sup>Fopx3<sup>-</sup> population in the brain of *Foxp3<sup>Cre</sup>IL27<sup>fl/fl</sup>* mice and WT littermates 21 d after EAE induction. Each symbol represents an individual mouse ( $n = 5$  for *Foxp3<sup>Cre</sup>IL27<sup>+/+</sup>* and 9 for *Foxp3<sup>Cre</sup>IL27<sup>fl/fl</sup>*). **f,** The disease severity scored regularly based on clinical symptoms.

Each symbol represents the average of mice from two independent experiments ( $n = 5$  for  $Foxp3^{Cre}II27^{+/+}$  and 11 for  $Foxp3^{Cre}II27^{fl/fl}$ ). Data are presented as mean values  $\pm$  s.d. In **a**, \*\*\*\* $P < 0.0001$ . In **b**, NS = 0.0944. In **c**, \* $P = 0.0203$  (day 18), 0.0220 (day 19), 0.0044 (day 20) and 0.0077 (day 21). In **d**, NS = 0.5026. In **e**, NS = 0.2346. Statistical significance was determined using a two-tailed, unpaired Student's *t*-test.

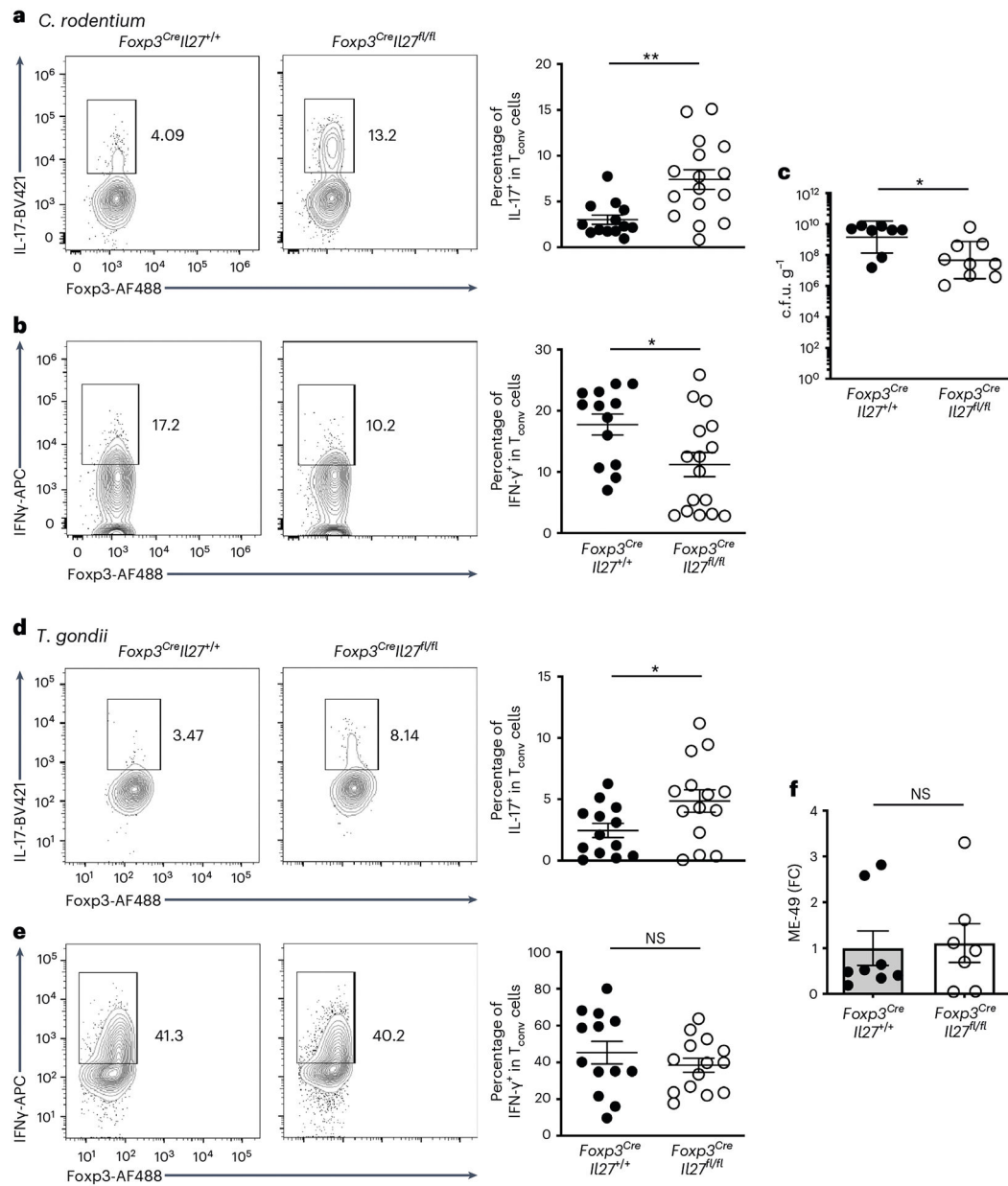


**Fig. 6 | Enhanced IL-17 responses in mice with T<sub>reg</sub> cell-specific IL-27 ablation selectively helped protect against enteric bacterial infection.**

**a,b**, FACS analysis and frequencies of IL-17<sup>+</sup> (**a**) and IFN-γ<sup>+</sup> (**b**) T<sub>conv</sub> cells gated on the live CD4<sup>+</sup>Foxp3<sup>-</sup> population in LI LP of  $Foxp3^{Cre}Il27^{fl/fl}$  mice and WT littermates at day 10 post-*C. rodentium* infection. Each symbol represents an individual mouse ( $n = 13$  for  $Foxp3^{Cre}Il27^{+/+}$  and 16 for  $Foxp3^{Cre}Il27^{fl/fl}$ ). **c**, Enumeration of *C. rodentium* in the LI of  $Foxp3^{Cre}Il27^{fl/fl}$  mice and WT littermates at day 10 post-*C. rodentium* infection. Each symbol represents an individual mouse ( $n = 8$  for  $Foxp3^{Cre}Il27^{+/+}$  and 9 for  $Foxp3^{Cre}Il27^{fl/fl}$ ). **d,e**, FACS analysis and frequencies of IL-17<sup>+</sup> (**d**) and IFN-γ<sup>+</sup> (**e**) T<sub>conv</sub> cells gated on the live CD4<sup>+</sup>Foxp3<sup>-</sup> population in SI LP of  $Foxp3^{Cre}Il27^{fl/fl}$  mice and WT littermates at day 8 post-*T. gondii* infection. Each symbol represents an individual mouse ( $n = 13$  for  $Foxp3^{Cre}Il27^{+/+}$  and 14 for  $Foxp3^{Cre}Il27^{fl/fl}$ ). **f**, The qPCR analysis of parasite burden in SI

of *Foxp3<sup>Cre</sup>Il27<sup>fl/fl</sup>* mice and WT littermates at day 8 post-*T. gondii* infection. Each symbol represents an individual mouse ( $n = 8$  for *Foxp3<sup>Cre</sup>Il27<sup>+/+</sup>* and 7 for *Foxp3<sup>Cre</sup>Il27<sup>fl/fl</sup>*). Data are presented as mean values  $\pm$  s.d. In **a**,  $**P = 0.0013$ . In **b**,  $*P = 0.0187$ . In **c**,  $*P = 0.0221$ . In **d**,  $*P = 0.0368$ . In **e**, NS = 0.3574. In **f**, NS = 0.8449. Statistical significance was determined using a two-tailed, unpaired Student's *t*-test.



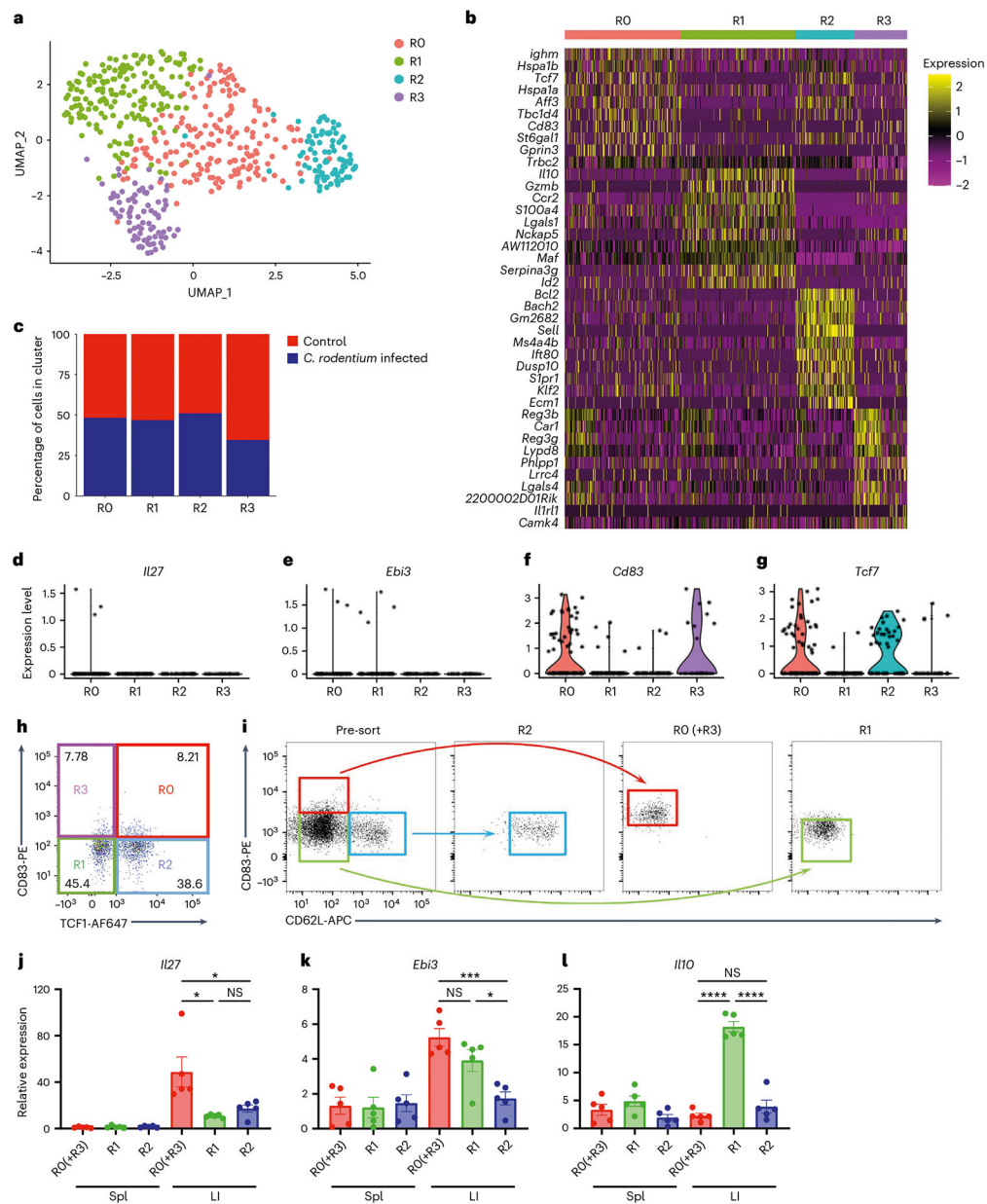


**Fig. 7 | Single-cell analyses identify a putative IL-27-producing  $T_{reg}$  cell subset in the inflammatory intestinal tissue.**

**a**, UMAP plots of intestinal  $T_{reg}$  cell clusters, colored by cluster identity. **b**, Heatmap of the top ten DEGs between each intestinal  $T_{reg}$  cell cluster. **c**, Percentage of cells within each intestinal  $T_{reg}$  cell cluster from mice with or without *C. rodentium* infection. **d–g**, Violin plots of *Il27* (**d**), *Ebi3* (**e**), *Cd83* (**f**) and *Tcf7* (**g**) in different intestinal  $T_{reg}$  cell clusters from *C. rodentium*-infected mice. **h**, FACS analysis of intestinal  $CD4^+Foxp3^+$   $T_{reg}$  cell clusters based on the expression of CD83 and TCF1. **i**, Representative FACS profiles with gating strategy for isolating different intestinal  $T_{reg}$  cell subsets based on the expression of CD83 and CD62L. **j–l**, The qPCR analyses for the expressions of *Il27* (**j**), *Ebi3* (**k**) and *Il10* (**l**) in different  $T_{reg}$  cell subsets in spleen (Spl) or LI LP from *C. rodentium*-infected mice. Each

symbol represents a FACS-isolated cell sample pooled from three mice ( $n = 5$ ). Data are presented as mean values  $\pm$  s.d. In **j**,  $*P = 0.0441$  (up) and  $0.0186$  (bottom left), and NS =  $0.0806$  (bottom right). In **k**,  $***P = 0.0005$  (up), NS =  $0.1380$  (bottom left) and  $*P = 0.0178$  (bottom right). In **l**, NS =  $0.2260$  (up), and  $****P < 0.0001$  (bottom left) and  $< 0.0001$  (bottom right). Statistical significance was determined using a two-tailed, unpaired Student's  $t$ -test.